Validation of the version 4.5 MAESTRO ozone and NO_2 measurements

Paul S. Jeffery[1], James R. Drummond[2], C. Thomas McElroy[3], Kaley A. Walker[1], and Jiansheng Zou[1]

[1]Department of Physics, University of Toronto, Toronto, ON, M5S 1A7, Canada
[2]Department of Physics and Atmospheric Physics, Dalhousie University, Halifax, NS, Canada
[3]Department of Earth and Space Science and Engineering, York University, Toronto, ON, M3J 1P3, Canada

Correspondence: Kaley A. Walker (kaley.walker@utoronto.ca)

Abstract. Launched aboard the Canadian satellite SCISAT in August 2003, the Measurement of Aerosol Extinction in the Stratosphere and Troposphere Retrieved by Occultation (MAESTRO) instrument has been measuring solar absorption spectra in the ultraviolet (UV) and visible part of the spectrum for more than 20 years. The UV channel measurements from MAESTRO are used to retrieve profiles of ozone from the short-wavelength end of the Chappuis band (UV-ozone) and NO_2, while measurements made in the visible part of the spectrum are used to retrieve a separate ozone (Vis.-ozone) product. The latest ozone and NO_2 profile products, version 4.5, have been released, which initially cover the period from February 2004 to December 2023 and which will continue to be updated. The version 4.5 retrieval algorithm represents an improvement from previous versions, with changes including updated pressure and temperature input information, an improved algorithm for high-sun reference spectrum calculation, improved Rayleigh scattering modeling, and the change to a Twomey-Tikonov inversion algorithm from a Chahine relaxation technique. Due to the buildup of an unknown contaminant, the UV-ozone and NO_2 products are only viable up to June 2009 for NO_2 and December 2009 for UV-ozone. This study presents comparisons of the version 4.5 MAESTRO ozone and NO_2 measurements with coincident, both spatially and temporally, measurements from an ensemble of 11 other satellite limb-viewing instruments. In the stratosphere, the Vis.-ozone product was found to possess a small high bias, with stratosphere-averaged relative differences between 2.3 % and 8.2 %, but overall good agreement with the comparison datasets is found. A similar bias, albeit with slightly poorer agreement, is found with the UV-ozone product in the stratosphere, with the average stratospheric agreement between MAESTRO and the other datasets ranging from 2.8 % to 11.9 %. For NO_2, general agreement with the comparison datasets is only found in the range from 20 to 40 km. Within this range, MAESTRO is found to have a low bias for NO_2, and most of the datasets agree to within 27.2 %, although the average agreement ranges from 8.5 % to 43.4 %.

1 Introduction

Ozone is one of the most important trace gas species in the atmosphere due to its role in absorbing solar ultraviolet (UV) radiation. Specifically, the absorption of UV radiation by the stratospheric ozone layer protects terrestrial life on Earth from the harmful effects of this radiation, while also giving rise to the thermal structure and stability of the stratosphere through the release of the absorbed radiant energy as heat (Jacob, 1999; Brasseur and Solomon, 2005). Throughout the twentieth century,

emissions of ozone-depleting substances (ODSs) diminished concentrations of stratospheric ozone, leading to drastic effects such as Arctic and Antarctic ozone holes (Lacis et al., 1990; Brasseur and Solomon, 2005; Manney et al., 2011). While the 1987 Montreal Protocol and its subsequent amendments phased out the use of ODSs, ozone recovery is a complicated process requiring in-depth understanding of changes in the distribution of ozone throughout the atmosphere. Currently, only satellite-based observations are capable of providing the high-resolution measurements required for detailed analyses of ozone's distribution, and the changes thereof, with sufficient global and temporal coverage.

One such instrument that has been used to make measurements of ozone, as well as nitrogen dioxide (NO_2) which participates in catalytic reactions that destroy ozone, is the Measurement of Aerosol Extinction in the Stratosphere and Troposphere Retrieved by Occultation (MAESTRO; McElroy et al., 2007). MAESTRO is a dual UV-visible spectrometer that operates in a limb-viewing geometry as one of the two instruments of the Atmospheric Chemistry Experiment (ACE) mission, alongside the ACE Fourier Transform Spectrometer (ACE-FTS; Bernath et al., 2005; Bernath, 2017). The ACE mission, aboard the Canadian SCISAT satellite, has a primary objective of studying the chemical and dynamical processes that impact the distribution of upper tropospheric and stratospheric ozone. Emphasis is placed on ozone in the Arctic, and so the latitudinal coverage of the ACE instruments focus on the polar regions, though due to the inclination of SCISAT's orbit over the course of a year coverage spans from 85°N to 85°S, taking approximately three months to cover this entire range. As the two ACE instruments employ the solar occultation technique to measure solar absorption spectra, measurements are made only during sunrise and sunset, as viewed by the instrument. Up to 15 sunrises and 15 sunsets can be measured per day.

The UV channel measurements from MAESTRO are used to retrieve profiles of ozone from the short-wavelength end of the Chappuis band and NO_2, while measurements made with the visible (Vis.) channel are used to retrieve a separate ozone product from the Chappuis band. The two ozone products are deemed the UV-ozone and Vis.-ozone products. Since early in its mission, MAESTRO has been affected by the buildup of an unknown contaminant, which has affected the ability to retrieve trace gas profiles from its UV measurements and since 2015 very little light with wavelength shorter than 500 nm is transmitted through the instrument (Sioris et al., 2016; Bernath, 2017). As a result, the NO_2 product is only viable from the start of the mission to the end of June 2009, and the UV-ozone product is viable only until the end of December 2009. The Vis.-ozone measurements remain operational through to the present.

Satellite measurements must be validated against measurements from other instruments in order to ensure they are well characterized and to determine any biases that exist between datasets. Additionally, by validating their biases these datasets are able to be incorporated into further cross-validation and merged series records. Recently, a new version of the MAESTRO ozone and NO_2 products, version 4.5, has been made publicly available (https://databace.scisat.ca/level2/; access requires registration) and, as with prior versions of these products, they must be validated to ensure the continuity of data series quality (e.g., Dupuy et al., 2009; Adams et al., 2012; Bognar et al., 2019). The focus of this work is on the comparison of these new version 4.5 MAESTRO trace gas measurement products against coincident measurements from an ensemble of other limb sounding instruments. The choice to focus on limb sounders is due to their vertical resolution being higher than what is found with nadir-viewing instruments.

Table 1. Summary of the spatial and temporal coverage of the instruments used in this study, along with the trace gas species used here from each, the data version for the products employed, and the measurement technique of each instrument.

Instrument	Gas species used	Data version	Measurement Period	Latitudinal coverage	Observation method
MAESTRO	O_3, NO_2	4.5	2004–present	85° N to 85° S	Solar occultation
ACE-FTS	O_3, NO_2	4.1/4.2, 5.2	2004–present	85° N to 85° S	Solar occultation
OSIRIS	O_3, NO_2	7.2	2001–present	82.5° N to 82.5° S	Limb scatter
Odin-SMR	O_3	3.0	2001–present	82.5° N to 82.5° S	Limb emission
GOMOS	O_3, NO_2	IPF 6.01	2002–2012	90° N to 90° S	Stellar occultation
MIPAS	O_3, NO_2	IMK-IAA 8_261	2002–2012	90° N to 90° S	Limb emission
SCIAMACHY	O_3, NO_2	IUP 3.5	2002–2012	85° N to 85° S	Limb scatter
Aura-MLS	O_3	5.3	2004–present	82° N to 82° S	Limb emission
OMPS-LP	O_3	NASA 2.6	2012–present	81.5° N to 81.5° S	Limb scatter
SAGE II	O_3, NO_2	7.0	1984–2005	80° N to 80° S	Solar occultation
SAGE III/M3M	O_3, NO_2	4	2001–2005	30° S to 60° S (sunrise), 80° N to 45° N (sunset)	Solar occultation
SAGE III/ISS	O_3	5.3	2017–present	70° N to 70° S	Solar occultation

This paper is organized as follows; Sect. 2 presents an overview of the MAESTRO instrument, as well as the comparison instruments used in this study, while Sect. 3 discusses the comparison methodology. The results are presented in Sect. 4, with Vis.-ozone presented in Sect. 4.1, the UV-ozone in Sect. 4.2, and NO_2 in Sect. 4.3. Finally, a summary is presented in Sect. 5.

2 MAESTRO and comparisons instruments

In this section, the MAESTRO instrument and the comparison ozone and NO_2 instruments used in this study are presented. The instruments are grouped by their measurement platforms, with the relevant information about the platform detailed in brief ahead of their corresponding instrument(s). Key details, including the data version, measurement technique, and the spatial and temporal coverage of these instruments are presented in Table 1.

2.1 Atmospheric Chemistry Experiment

The ACE mission, aboard the Canadian satellite SCISAT, was launched into a circular low-Earth orbit (650 km altitude, 74° inclination) on 12 August 2003 (Bernath et al., 2005). As discussed above, aboard SCISAT are two instruments: MAESTRO and ACE-FTS.

2.1.1 MAESTRO

The MAESTRO instrument aboard SCISAT is composed of a pair of grating spectrophotometers that record spectra between 285 and 1030 nm with a wavelength-dependent resolution of 1–2 nm (McElroy et al., 2007). The solar occultation measurements made by MAESTRO consist of sequences of 60 spectra taken between the cloud tops and 100 km above the surface, as well as an additional 20 spectra taken between 100 and 150 km for use as reference spectra. The 1.2 km field-of-view (FOV) of MAESTRO on the limb, combined with typical measurement spacing of around 1 to 2 km, leads to an effective vertical resolution for MAESTRO of 1–2 km. Scientific operation of MAESTRO commenced in February 2004 and continues through to the present, despite the build-up of an unknown contaminant blocking the transmission of light with wavelengths shorter than 500 nm (Sioris et al., 2016; Bernath, 2017).

For the newest version of the MAESTRO products, version 4.5, measurements made by MAESTRO are used to retrieve volume mixing ratio (VMR) profiles of UV-ozone, NO_2, Vis.-ozone, and optical depth. As with previous versions of the MAESTRO products, the general retrieval is based on a two-step approach wherein a modified differential optical absorption spectroscopy (DOAS) technique is used to obtain line-of-sight column densities at each measurement tangent height (McElroy et al., 2007; Kar et al., 2007; Bognar et al., 2019). However, unlike previous versions, a Twomey-Tikonov inversion algorithm is used to invert these slant columns into VMR profiles. In the version 4.5 retrieval algorithm, the Vandaele et al. (2002) NO_2 and Serdyuchenko et al. (2011) ozone cross-sections are employed, and the retrieval includes a temperature correction based on the temperature-dependence of the ozone cross-sections. The new version 4.5 retrieval also incorporates improved Rayleigh scattering modeling and an improved algorithm for high-sun reference spectrum calculation. The retrieval is performed on an altitude grid spanning from 5 to 80 km; however the profile is provided on a grid spanning 0 to 100 km, extrapolating from the retrieved profile to the rest of the grid. Above 50 km, the data should be used with caution as the retrieval is less constrained. As with previous versions of the MAESTRO retrieval, the version 4.5 inversion uses the ACE-FTS pressure and temperature profile data, however this has been updated to use the ACE-FTS version 5.2 data, which addresses the possibility of a drift in the MAESTRO products produced using the ACE-FTS version 3.5/3.6 data that results from systematic CO_2 modeling errors discussed in Sheese et al. (2022). The version 4.5 dataset used covers the period from February 2004 to December 2023.

Before release, extreme outliers are removed from the MAESTRO dataset by filtering out profiles of ozone in which the maximum VMR between 5 and 50 km is greater than 30 ppmv or less than 0.01 ppmv, and similarly filtering out NO_2 profiles whose maximum VMR is greater than 20 ppbv or less than 0.01 ppbv over this same vertical range. In this study, in order to further screen the released MAESTRO version 4.5 data for any remaining outliers, four steps are taken. First, the UV products are only used up to their recommended end dates, specifically the end of June 2009 for NO_2, and the end of December 2009 for UV-ozone. Second, the most extreme outliers, which usually occur near the top of the MAESTRO profile where the retrieval is less constrained, are removed by filtering out values in excess of 500 ppmv for ozone or 500 ppbv for NO_2. Third, incomplete profiles, spanning less than 40 km in the vertical, are removed as they have been found to be poorly constrained by the MAESTRO retrieval algorithm. Fourth, the remaining data is screened with a 10 median absolute deviation (MAD) filter, with all VMR values more than 10 MAD away from the median at each altitude removed from the analysis. Excluding the

date-based filters, this method of filtering removed <0.1 % of the MAESTRO Vis.-ozone profiles, <0.1 % of the MAESTRO UV-ozone profiles, and <0.1 % of the MAESTRO NO_2 profiles.

2.1.2 ACE-FTS

The other instrument aboard SCISAT, ACE-FTS, is a Fourier transform spectrometer measuring the spectral range between 750–4400 cm^{-1} with 0.02 cm^{-1} spectral resolution (Bernath et al., 2005). ACE-FTS records solar absorption spectra at tangent heights spanning from the cloud tops to 150 km, with vertical spacing between 1.5 and 6 km and a vertical FOV of 3 to 4 km on the limb. As with MAESTRO, scientific operations of ACE-FTS commenced in February 2004 and continue through to the present.

The measurements made by ACE-FTS are used to retrieve vertical profile information about temperature, pressure, and VMR for several dozen trace gas species. The full retrieval process is described in Boone et al. (2005, 2013, 2020, 2023), but in brief involves establishing pressure and temperature profiles using the operational global weather assimilation and forecasting system managed by the Meteorological Service of Canada (Buehner et al., 2015) below approximately 18 km and through analysis of CO_2 spectral lines above this altitude, and then using a global Levenberg-Marquardt nonlinear least squares fitting algorithm in order to determine VMR profiles with 3–4 km vertical resolution. In this work, two versions of the ACE-FTS profiles of ozone and NO_2 are used; the version 4.1/4.2 profiles, which have undergone prior validation efforts, and the new version 5.2 profiles, which expand the list of retrieved products from ACE-FTS measurements, contribute the pressure and temperature information used in the MAESTRO retrievals, and which are considered the current working product (Boone et al., 2023). The ACE-FTS data used in this study cover the period from February 2004 to December 2023.

Quality flags have been developed for the ACE-FTS version 4.1/4.2 and version 5.2 products, which have been applied to the datasets from ACE-FTS used in this work (Sheese et al., 2015). As recommended, all measurements marked with quality flags >0 are removed in order to filter out extreme outliers.

The ACE-FTS version 4.1/4.2 profiles of NO_2 have been compared against coincident measurements from OSIRIS by Dubé et al. (2022), and against SAGE III/ISS by Strode et al. (2022). The former found that ACE-FTS NO_2 is smaller than that from OSIRIS by approximately 20 % at 18 km, larger than OSIRIS by about 10 % between 25 and 30 km, and again smaller than OSIRIS by approximately 20 % at 38 km, while the latter found ACE-FTS NO_2 to be less than that of SAGE III/ISS by between 10 and 20 % over the stratosphere, with better agreement at lower altitudes. Strode et al. (2022) also compared ACE-FTS ozone against that from SAGE III/ISS, and found ACE-FTS ozone to be about 5 % larger than that of SAGE III/ISS at 15 km, but within approximately 0–2 % up to about 45 km. Sheese et al. (2022) compared the version 4.1/4.2 ozone to measurements from MAESTRO, OSIRIS, Aura-MLS, SABER, and Odin-SMR, and found that the weighted average difference showed ACE-FTS ozone was larger than these other datasets by between 2 and 9 % over the stratosphere, with the largest differences occurring around 30 km.

2.2 Odin

The Odin satellite was launched into a near-circular Sun-synchronous low-earth orbit (600 km, 98° inclination) in February 2001 (Murtagh et al., 2002). The ascending (descending) node of Odin has drifted over time from 18:00 (6:00) local time to an hour later, and then back to only half an hour later, due to a slight procession in its orbit (Llewellyn et al., 2004; Bourassa et al., 2014). Odin was designed for a mixed aeronomy/astronomy mission, splitting time between observation modes designed for each focus; however, since May 2007 Odin has solely made atmospheric observations. Aboard Odin are two main instruments; the Sub-Millimetre Radiometer (Odin-SMR) and the Optical Spectrograph and InfraRed Imaging System (OSIRIS).

2.2.1 Odin-SMR

Odin-SMR instrument employs four tunable sub-millimeter radiometers that measure thermal limb emission in the 486–581 GHz spectral region, along with a millimeter radiometer that measures thermal emission around 119 GHz (Murtagh et al., 2002; Urban et al., 2005). Two auto-correlator spectrometers generate spectra from the observed signal with 800 MHz bandwidth and 2 MHz resolution; however, only two channels can be measured simultaneously. Under its typical stratospheric observation mode, Odin-SMR measures in two frequency bands centered at 501.8 and 544.6 GHz. During measurements, Odin-SMR scans from 7 km to between 70 and 110 km, depending on its observation mode, with an approximately 2 km FOV on the limb, 1.5 km vertical measurement spacing below 50 km and 6 km spacing above this altitude (Murtagh et al., 2002, 2020). Stratospheric observations are made every two days (every three days prior to May 2007), and approximately 900 profiles are recorded per day. Scientific operations of Odin-SMR began in July 2001 and continue through to the present.

The measurements from Odin-SMR are used to retrieve VMR profiles of several trace gas species, as well as temperature. Eriksson (2020) details the retrieval, which involves using the optimal estimation method with a Levenberg–Marquardt iteration scheme to retrieve profiles on measurement-tangent-point pressure levels. Estimates of geometrical altitude are provided alongside the retrieved products. The products retrieved vary with the Odin-SMR observation mode, and currently multiple ozone products are produced from three separate channels. In this study, the version 3.0 ozone product from the 544.6 GHz channel is used, as recommended by Murtagh et al. (2020) and Pérot et al. (2020). While this ozone product spans from 11 to 109 km, the valid range is from 17 to 77 km. The vertical resolution of these profiles is 2–3 km over the valid range. The version 3.0 Odin-SMR data used in this study cover the period from February 2004 to September 2022.

These data are screened for quality control before being released. The two filters applied require a minimum value for the Levenberg–Marquardt damping parameter below 2 and that the spectral fit residuals are less than 1.5 K (Pérot et al., 2020). No further filtering is applied in this study to the Odin-SMR products.

The version 3.0 ozone retrieved from the 544.6 GHz channel has been previously compared to other coincident measurements in Murtagh et al. (2020) and Sheese et al. (2022). In the former, Odin-SMR ozone was compared against that of OSIRIS, MIPAS, and Aura-MLS. They found that Odin-SMR ozone was on average about 10–15 % smaller than MIPAS and OSIRIS between 20 and 50 km, and about 5–10 % smaller than MLS over this same range. Comparisons against ACE-FTS by Sheese et al. (2022) showed that Odin-SMR ozone is low biased by about 5–10 %.

2.2.2 OSIRIS

OSIRIS consists of a grating optical spectrograph (OS) and an infrared imager (IRI). The former records Rayleigh- and Mie-scattered sunlight spectra between 280–810 nm with 1–2 nm resolution, while the latter measures airglow (Llewellyn et al., 2004). OSIRIS records limb-radiance at tangent heights between 7 and 70 km under its typical (stratospheric) operation mode, with altitude-dependant vertical spacing of 1 to 2 km and a vertical FOV on the limb of about 1 km (Haley et al., 2004). Between 30 and 60 profiles are recorded every orbit, with 15 orbits completed per day. Due to the orbital geometry of Odin, coverage focuses on the southern hemisphere between October and February and the northern hemisphere between March and September. Routine operation of OSIRIS began in November 2001 and continues through to the present.

Limb-radiance profiles recorded by OSIRIS are used to retrieve profiles of ozone, $\mathrm{NO_2}$, and sulphate aerosol from the cloud tops to 60 km (Degenstein et al., 2009). Details of the version 7.2 $\mathrm{NO_2}$ and ozone retrievals, used in this study, can be found in Dubé et al. (2022) and Bognar et al. (2022) respectively. Broadly, these retrievals employ a Levenberg–Marquardt algorithm to retrieve number density profiles of these two species using pressure and temperature data from the Modern-Era Retrospective analysis for Research and Applications Version 2 (MERRA-2; Gelaro et al., 2017).These products have a vertical resolution of 1.5 km for ozone and 2–3 km for $\mathrm{NO_2}$, In this study, the reported number density values are converted into VMRs using the MERRA-2 temperature and pressure information used in the retrievals. The OSIRIS data used in this study cover the period from February 2004 to December 2023.

The OSIRIS data are screened for quality control ahead of release. The involves screening the limb radiance measurements for clouds or cosmic rays (Bognar et al., 2022). The $\mathrm{NO_2}$ product is further filtered through the application of an averaging-kernel-based criterion for determining the functional lower bound of the retrieved product (Dubé et al., 2022). No further data filtering was applied in this study.

Dubé et al. (2022) compared version 7.2 OSIRIS $\mathrm{NO_2}$ with that from ACE-FTS and SAGE III/ISS. They found that OSIRIS $\mathrm{NO_2}$ was larger than that of ACE-FTS around the tropopause in the northern hemisphere, with differences as large as 50 %, as well as above 35 km, with differences of 10–20 %, whereas elsewhere ACE-FTS had larger $\mathrm{NO_2}$ values by about 10 %. Compared to SAGE III/ISS the OSIRIS product was found to be smaller over virtually all of the upper troposphere and stratosphere, albeit with better agreement found at higher altitudes. The average difference of these comparisons throughout the stratosphere is about 20 %. Similar results were found by Strode et al. (2022) for $\mathrm{NO_2}$. Strode et al. (2022) also found version 7.2 OSIRIS ozone to be within about 5 % of SAGE III/ISS over much of the stratosphere, with larger differences, of 10–15 %, found below 20 km.

2.3 Envisat

The ENVIronmental SATellite (Envisat) was launched into a sun-synchronous low-earth orbit (800 km, 98.55° inclination) in February 2002 (Bertaux et al., 2010). Envisat had an ascending (descending) node at 22:00 (10:00) local time, and operated until April 2012 when contact was lost with the satellite. Aboard Envisat were the Global Ozone Monitoring by Occultation

of Stars (GOMOS), Michelson Interferometer for Passive Atmospheric Sounding (MIPAS), and Scanning Imaging Absorption spectroMeter for Atmospheric CHartographY (SCIAMACHY) instruments.

2.3.1 GOMOS

The GOMOS instrument was composed of a pair of grating spectrometers operating in the UV-visible, between 248–690 nm with 0.8 nm resolution, and the infrared (IR), between 750–776 nm and 916–956 nm with 0.13 nm resolution, along with a pair of photometers (Kyrölä et al., 2004; Bertaux et al., 2010). GOMOS measured atmospheric transmission spectra using a stellar occultation technique, using about 180 stars as light sources and making measurements from between 5 and 20 km, depending on the presence of clouds and the brightness of the reference star, to 150 km (Tamminen et al., 2010). Measurements were spaced by 0.5 to 1.6 km, and were recorded during both the night (dark limb) and day (bright limb) as viewed by the instrument. About 600 occultations were recorded per day, with 100–200 of those being dark limb measurements. Scientific operation of GOMOS began in March 2002 and ended in April 2012.

GOMOS stellar occultation measurements are used to retrieve vertical profiles of five trace gases, as well as aerosols. As detailed in Kyrölä et al. (2010), the UV-visible retrievals, which produce the ozone and NO_2 products, use a maximum likelihood method to obtain tangent column densities, which were then inverted using Tikhonov regularization to determine number density profiles, with the inversion set up to produce profiles at a desired vertical resolution. For ozone the vertical resolution is 2 km below 30 km, increasing to 3 km at and above 40 km, while for the other products the vertical resolution is 4 km (Kyrölä et al., 2010; Tamminen et al., 2010). The air density estimates required for this come from the European Centre for Medium-Range Weather Forecasts (ECMWF) 24 h forecast below 1 hPa, and from the MSIS-90 model (Hedin, 1991) above 1 hPa. The Instrument Processing Facility (IPF) version 6.01 GOMOS retrieval products are used in this study, which are made available on a uniform 1 km vertical grid, and the number density profiles are converted into VMR profiles using the air density profiles used for the retrieval. The GOMOS data used in this study cover the period from February 2004 to April 2012.

The GOMOS product quality is impacted by the brightness of the target star used for occultations. Following product usage recommendations, only those ozone measurements made using stars that reliably produce viable results have been used in this work (Kyrölä et al., 2017). The ozone product is also provided with quality flags that identify the presence of outliers in the stratosphere and all profiles flagged with a stratospheric outlier have been filtered from analysis. Additionally, it has been found that the bright limb occultations are affected strongly by scattered solar light and so only the dark limb measurements are used in this study. Beyond this, measurement-specific altitude validity ranges are provided for each gas, and only data within this range are included in this study (Kyrölä et al., 2017). Finally, a 10 MAD filter is applied to the GOMOS data, removing all VMR values more than 10 MAD away from the median at each altitude.

GOMOS IPF version 6 ozone and NO_2 profiles have previously been compared in Adams et al. (2014) and Sheese et al. (2016) respectively. The former found the GOMOS ozone product is within approximately 2.5 % of that from OSIRIS between 20 and 50 km, but below 20 km the GOMOS product is over 20 % larger than that of OSIRIS. Sheese et al. (2016) found that ACE-FTS agreed with GOMOS NO_2 to within 20 % between about 23 and 40 km, with ACE-FTS showing less NO_2 at lower

altitudes, and more NO_2 above approximately 27 km. Climatological comparisons by Hegglin et al. (2021) found IPF version 6.01 GOMOS ozone is lower than that from a multi-instrument mean (MIM) by more than 20 % near the tropopause, and by between 0 and 10 % over most of the stratosphere.

2.3.2 MIPAS

MIPAS was a Fourier transform spectrometer aboard Envisat that measured limb emission spectra over five mid-IR bands between 685–2410 cm^{-1} (Fischer et al., 2008). Between July 2002 and March 2004, MIPAS was operated at its full spectral resolution, 0.035 cm^{-1}, however instrument subsystem issues led to a gap in measurements between April and December 2004, after which time it was operated at a reduced resolution of 0.0625 cm^{-1} (Kiefer et al., 2023). MIPAS had a 3 km vertical FOV, and during the full resolution period made measurements between 6 and 68 km with 3 to 6 km spacing, producing about 1000 observations per day. While operated at reduced resolution, nominal operations involved MIPAS measuring between 6 and 70 km with 1.5 to 4 km spacing, making approximately 20 % more measurements per day than during full resolution operation (Fischer et al., 2008; von Clarmann et al., 2009). Scientific operation of MIPAS ended in April 2012.

Limb emission spectra recorded by MIPAS are used to retrieve profiles of temperature and over two dozen trace gases. Different MIPAS retrievals are performed at multiple institutions, and this study employs that produced by the Institut für Meteorologie und Klimaforschung (IMK) in collaboration with the Instituto de Astrofísica de Andalucía (IAA). Compared to the MIPAS retrievals from other institutions, the ozone product from the IMK-IAA retrieval has been found by Laeng et al. (2017) to be less biased by a factor of two. The IMK-IAA retrieval is described in Funke et al. (2001), von Clarmann et al. (2003, 2009), and Kiefer et al. (2021), and is based on multi-parameter fitting of spectra using Tikhonov regularization. Briefly, temperature profiles are retrieved and the tangent height pressures are determined using the hydrostatic equation. Then trace gas species are retrieved using these profiles, first for species with major contributions to the IR spectra, including ozone and NO_2, and then for all remaining species. In this study, the version 8 IMK-IAA products from the reduced resolution period measured in the nominal operation mode (version 8_261) are used, with no data used from the full resolution MIPAS period as only six weeks of overlap are found with MAESTRO. This ozone product has a vertical resolution of about 3–4 km, while the NO_2 product has a vertical resolution of 3–6 km, increasing with altitude in the stratosphere. The MIPAS data used in this study cover the period from November 2004 to April 2012.

Adapting the work of Funke et al. (2023), the MIPAS IMK-IAA data used in this study are screened for quality through analysis of the reduced χ^2 of the retrieval fit; specifically by filtering out any profile whose reduced χ^2 is equal to or larger than 5. Following this, data were only used if the visibility marker included with the data was set to 1 for a given tangent altitude, indicative of a cloud-free observation at that altitude.

Prior versions of the MIPAS IMK-IAA ozone and NO_2 products have been validated against sets of coincident measurements from other instruments. Version 5 MIPAS ozone was found by Sheese et al. (2017) to agree with ACE-FTS to within 5 % between 10 and 45 km, above which MIPAS was found to yield less ozone by about 10–20 % up to about 60 km. They also found agreement for MIPAS ozone to within about 5 % of Aura-MLS, up to about 60 km. Recent climatology studies of the version 5 MIPAS ozone found that in comparisons against a MIM, MIPAS was within 5 % over much of the stratosphere,

only showing significantly poorer agreement around the tropopause (Hegglin et al., 2021). Comparisons of the version 5 NO_2 from MIPAS against ACE-FTS showed the former to yield less NO_2 below 30 km, by about 30 %, above which it yielded increasingly more NO_2 with altitude, reaching differences in excess of 60 % (Sheese et al., 2016). Better agreement, to within about 10 %, was found between MIPAS NO_2 and both OSIRIS and SCIAMACHY below 30 km (Sheese et al., 2016).

2.3.3 SCIAMACHY

SCIAMACHY was a passive imaging grating spectrometer that measured within the spectral range between 240–2380 nm over eight channels, with channel-dependant spectral resolution between 0.24 and 1.48 nm (Burrows et al., 1995; Bovensmann et al., 1999). Designed for mixed operation, SCIAMACHY made limb scatter, nadir backscatter, and solar/lunar occultation measurements; however, only the results from the limb scatter measurements are used here. These limb scatter measurements were recorded at tangent altitudes from just below the surface up to about 92 km, with 3.3 km vertical spacing and a vertical FOV of about 2.6 km on the limb. About 1000 limb scatter measurements were made per day. Scientific operation of SCIAMACHY commenced August 2002 and continued through to April 2012.

Number density profiles are retrieved from the SCIAMACHY limb measurements for several species including ozone and NO_2. In this study, the version 3.5 scientific retrievals are used. These retrievals, described in detail in Jia et al. (2015) for ozone and Bauer et al. (2012) for NO_2, employ a DOAS technique and Tikhonov regularization to retrieve profiles of ozone between 8 and 65 km and of NO_2 between 10 and 45 km. Both species are retrieved on the measurement tangent height grid and the retrievals have a vertical resolution of 3–5 km. Pressure and temperature information for this retrieval come from ECMWF reanalysis, and are used here to convert the number density profiles into VMR profiles. The SCIAMACHY data used in this study cover the period from February 2004 to April 2012.

Following quality control measures from prior analysis of the SCIAMACHY measurement products (e.g., Gebhardt et al., 2014; SPARC-DI, 2017; Sofieva et al., 2021), data are filtered out if measured over the south Atlantic ocean (-20°S to -70°S, 0°W to 90°W) to remove the impact of the South Atlantic Anomaly. No further filtering is applied.

Profile comparisons of SCIAMACHY NO_2 against ACE-FTS by Sheese et al. (2016) showed that the SCIAMACHY version 3.1 product is low-biased below about 30 km, with relative differences decreasing from 70 % at about 15 km to 20 % at 25 km, above which the two sets of profiles agree to within 20 %. However, cross-comparisons in the same study showed that the SCIAMACHY profiles agreed with OSIRIS and MIPAS profiles to within about 15 % over most of the stratosphere. For the SCIAMACHY version 3.0 ozone product, Jia et al. (2015) found a difference of less than 10 % when compared against ozonesonde measurements between 20 and 30 km, with SCIAMACHY showing less ozone than the ozonesondes. Climatology-based comparisons of version 3.5 SCIAMACHY ozone against a MIM showed that in the stratosphere ozone concentrations from SCIAMACHY are higher than the mean by 0–10 % below 25 km, and lower by approximately the same amount above this altitude (Hegglin et al., 2021)

2.4 Suomi-NPP

Suomi National Polar-orbiting Partnership (Suomi-NPP) was launched into a sun-synchronous low-Earth orbit (834 km, 98.8° inclination) in October 2011 (Rault and Loughman, 2013). With an ascending (descending) node at 13:30 (1:30), Suomi-NPP is host to five instruments, including the Ozone Mapping and Profiler Suite (OMPS).

2.4.1 OMPS-LP

OMPS is composed of three sensors; a nadir total column mapper (NM), nadir profiler (NP), and a limb profiler (LP). The nadir sensors, not used in this study, measure UV backscatter radiation, while the OMPS-LP measures limb scattered radiation from 290–1000 nm with wavelength-dependant spectral resolution ranging from 1.5 nm in the UV to 40 nm at 1000 nm (Flynn et al., 2004; Jaross et al., 2014). OMPS-LP itself is a prism spectrometer that measures spectra from three vertical slits offset horizontally by 4.25° (250 km across track). Each slit spans 112 km in the vertical, to ensure coverage from 0 to 80 km, with approximately 1 km sampling and a 1.3 to 1.7 km vertical FOV. Two spectra are recorded simultaneously from each slit with different integration times to account for differences in spectral intensity, and approximately 2400 observations are made per day from each slit. Scientific operation of the OMPS-LP began in February 2012 and continues through to the present.

OMPS-LP measurements are used to derive profiles of ozone and aerosol extinction. The ozone retrieval, detailed in Rault and Loughman (2013) and Kramarova et al. (2018), involves normalizing the measured radiances with measurements made at 60.5 km for the UV and 40.5 km for the visible, constructing wavelength pairs or triplets, and applying a Tikhonov regularization to obtain an estimate for ozone number density profiles. The retrieved profiles span from the cloud tops, or 12.5 km, to 57.5 km, with about 1.8 km vertical resolution. Values are reported on a uniform 1 km grid along with the MERRA-2-derived temperature and pressure information used for the retrievals. These temperature and pressure fields are used to convert the number density profiles into VMR in this work. The version 2.6 ozone product is used in this study, which only uses measurements made by the central vertical slit of OMPS-LP due to stray light affecting the side channel measurements (Kramarova and DeLand, 2023). This dataset covers the period from February 2012 to December 2023.

The OMPS-LP ozone data are provided with a set of retrieval metrics and quality screening flags. Following the recommendations for the version 2.6 product in Kramarova and DeLand (2023), data were filtered out if the retrieval algorithm convergence was greater than 10, and the ozone product was only used if the number of retrieval iterations was between 2 and 7. As for the quality flags, data were filtered out if the polar mesospheric cloud (PMC) flag indicated the presence of PMCs that affected the measurements, if the ozone quality flag indicated a wavelength shift in the algorithm, or if the quality measurement vector flag indicated a poor quality profile.

The OMPS-LP version 2.5 ozone product has been validated by comparison with ACE-FTS, Aura-MLS, and OSIRIS by Kramarova et al. (2018). They found OMPS-LP ozone to be between 10–15 % lower than that of ACE-FTS, Aura-MLS, and OSIRIS between 12.5 and about 20 km, above which differences were generally around 5 % up to 30 km. Between 30 and 40 km the OMPS-LP version 2.5 product was found to be 10 % larger than that of OSIRIS, and 5 % larger than that of ACE-FTS and Aura-MLS. Finally, above 40 km OMPS-LP yielded progressively less ozone with altitude than the other instruments,

reaching differences of approximately 10–20 % at 50 km. Further comparisons by Strode et al. (2022) showed the version 2.5 OMPS-LP ozone data to be generally larger than SAGE III/ISS below 20 km and above 40 km, and smaller in between these two altitudes, but in general agreement overall to within 10 %.

2.5 Aura

The Aura satellite was launched into a sun-synchronous low-earth orbit (705 km, 98° inclination) in July 2004 (Waters et al., 2006). Aura has an ascending (descending) node at 13:45 (1:45), and is host to four instruments including the Aura Microwave Limb Sounder (Aura-MLS).

2.5.1 Aura-MLS

The Aura-MLS instrument is composed of seven radiometers that measure microwave thermal emission in five spectral regions corresponding to 118 GHz, 190 GHz, 240 GHz, 640 GHz, and 2.5 THz (Waters et al., 2006; Livesey et al., 2022). During operations, Aura-MLS scans the radiometer antennae through the limb of the atmosphere, from the surface to about 90 km, every 25 s, resulting in about 3500 observations per day. The vertical FOV on the limb of the radiometers varies from 1.5 to 6.5 km, and measurements are made with approximately 1 km vertical spacing. Scientific operations of Aura-MLS began in August 2004 and continue through to the present.

Measurements made by Aura-MLS are used to retrieve vertical profiles of temperature, geopotential height, and VMR of 15 trace gas species including ozone. This process, detailed in Waters et al. (2006) and Livesey et al. (2022), begins with establishing estimates of temperature and tangent pressure through analysis of O_2 and O_2 isotopologues, followed by establishing estimates of nine trace gas species, including ozone. Over multiple phases these estimates are refined, and following this the remaining meteorology and trace gas fields are determined. The retrievals use an optimal estimation approach, and the products are retrieved on fixed pressure surfaces, with six pressure levels per decade. The vertical resolution of the retrievals varies from 2.5 km in the lower stratosphere to 5 km in the upper stratosphere. In this study, version 5.3 of the Aura-MLS ozone product is used, which requires transformation from its native pressure vertical coordinate to an altitude coordinate. This is accomplished by interpolating Aura-MLS ozone profiles that are coincident with MAESTRO profiles (see Sect. 3 for coincidence criteria) onto the MAESTRO altitude grid using the ACE-FTS/MAESTRO pressure at each altitude for the interpolation. The Aura-MLS data used in this study cover the period from August 2004 to December 2023.

The version 5.3 Aura-MLS data files include several quality and retrieval-related fields necessary for screening the retrieved data. Following the recommendations of Livesey et al. (2022), the Aura-MLS ozone data used in this study have been filtered to remove any profiles with quality flags less than 1.0, showing poor radiance fits, with convergence values greater than 1.03, showing divergence from the expected radiance fit, and with negative precision estimates, which indicates a non-physical effect arising from the a priori. Additionally, only profiles with even status fields were included, which exclude data with questionable profiles or affected by the presence of clouds. Lastly, ozone data are only used from the pressure levels between 261 and 0.001 hPa which is the valid range for the ozone retrievals.

The Aura-MLS version 5.1 ozone profiles have been compared to coincident profiles from ACE-FTS in Sheese et al. (2022), who found over the stratosphere Aura-MLS ozone was approximately 5–10 % smaller than that of ACE-FTS. Wang et al. (2020) found Aura-MLS version 4.1 ozone is smaller than that of SAGE III/ISS by 0–5 % over most of the stratosphere, showing more ozone only above 45 km. Climatological studies of Aura-MLS version 4.2 ozone against a MIM show a slight negative bias over most of the stratosphere of 0–5 % (Hegglin et al., 2021)

2.6 ERBS

The Earth Radiation Budget Satellite (ERBS) was launched into a circular low-earth orbit (610 km, 57° inclination) in October 1984 (Mauldin III et al., 1985; McCormick, 1987). Despite several hardware failures, ERBS remained operational until it was decommissioned in August 2005 (Damadeo et al., 2013). Aboard ERBS was the Stratospheric Aerosol and Gas Experiment II (SAGE II) instrument.

2.6.1 SAGE II

SAGE II was a seven channel grating spectrometer that measured between 385–1020 nm (Mauldin III et al., 1985; McCormick, 1987). Measuring from the cloud tops to about 150 km, SAGE II recorded solar occultation measurements during sunrise and sunset with a 0.5 km vertical FOV on the limb. Rather than remain fixed on the Sun center, this FOV was scanned vertically across the Sun disk, allowing for multiple measurements to be made at approximately the same altitude (McCormick et al., 1989; Damadeo et al., 2013). This resulted in approximately 1 km vertical resolution. Scientific operations of SAGE II began in October 1984, and until July 2000 15 sunrise and 15 sunset measurements were made per day (Wang et al., 2002). After this date, a pointing problem led to a reduction in the number of daily measurements to about 16 in total per day. Scientific operations ceased in August 2005 when ERBS was decommissioned.

Measurements from SAGE II are inverted to yield profiles of ozone, aerosol, NO_2, and water vapour using the algorithm detailed in Chu et al. (1989) and Damadeo et al. (2013). Slant-path transmission profiles are calculated from the solar occultation measurements and are used to derive species-specific slant-path column densities using a least squares fit. These are inverted to generate vertical profiles using an onion peeling algorithm. This process requires temperature and pressure data, which come from the Modern-Era Retrospective analysis for Research and Applications (MERRA; Rienecker et al., 2011) up to 0.1 mbar, above which the lapse rate from the Global Reference Atmospheric Model-1995 (GRAM-95; Justus and Johnson, 1997) is used. In this study, the version 7.0 SAGE II products are used, which span from the cloud top to 70 km for ozone, and up to 50 km for NO_2, and which are provided on a uniform 0.5 km grid. Air density data used in the retrieval are employed to convert the number density profiles into VMR. The SAGE II data used in this study cover the period from August 2004 to August 2005.

The SAGE II ozone data was screened for outliers using the retrieval uncertainty estimates and the aerosol extinction values, following the recommendations of Wang et al. (2002) and Kremser et al. (2020). Screening with the former led to the exclusion of all ozone data points with an uncertainty estimate of over 300 %, all points below 35 km with an uncertainty estimate over 200 %, and all profiles with an uncertainty estimate of more than 10 % in the 30–50 km range. For the latter, data points were

excluded below the altitude at which an aerosol extinction value exceeded $0.006\,\mathrm{km}^{-1}$, as well as below the altitude where the $525\,\mathrm{nm}$ aerosol extinction value exceeded $0.001\,\mathrm{km}^{-1}$ if the ratio of the $525\,\mathrm{nm}$ to $1020\,\mathrm{nm}$ aerosol product fell below 1.4. In addition, the version 7.0 SAGE II product is provided with a cloud filter field, which denotes altitudes affected by the presence of clouds, and all data for both ozone and $\mathrm{NO_2}$ affected as such were removed.

The SAGE II version 7.0 ozone product has been previously validated by Hubert et al. (2016), who found that SAGE II ozone was generally within 4 % of coincident ozonesonde measurements between 20 and 40 km, but below 20 km, SAGE II underestimates ozone by 10–15 %. Adams et al. (2013) found similar results in comparing coincident SAGE II version 7.0 profiles with those from OSIRIS, with the two ozone datasets agreeing to within 5 % above about 15 km, below which differences increased to 10 %, with SAGE II version 7.0 generally yielding less ozone than OSIRIS. Climatological comparisons of SAGE II ozone against a MIM by Hegglin et al. (2021) suggest that SAGE II underestimates ozone across the entire stratosphere, however this difference is usually less than 5 %, increasing around the tropopause to 10–20 %. Finally, climatologies of SAGE II version 6.2 $\mathrm{NO_2}$ have also been compared to a MIM, and over most of the stratosphere differences are within 20 %, with a low bias in the middle stratosphere and high bias above and below this (SPARC-DI, 2017).

2.7 Meteor-3M

The Meteor-3M satellite was launched into a sun-synchronous low-earth orbit (1020 km, 99.5° inclination) in December 2001 (Mauldin III et al., 1998; Thomason et al., 2010). The ascending (descending) node of the Meteor-3M was at 9:00 (21:00), and aboard the platform were several instruments including the Stratospheric Aerosol and Gas Experiment III/Meteor-3M (SAGE III/M3M). Meteor-3M operations ceased in March 2006 (Thomason et al., 2010).

2.7.1 SAGE III/M3M

The SAGE III/M3M instrument was composed of a grating spectrometer, which measured the spectral region from 280–1040 nm over 86 spectral channels, and a single photodiode that measured near 1550 nm (Mauldin III et al., 1998; Thomason et al., 2010). SAGE III/M3M made solar and lunar occultation measurements, though only the former are considered for this study due to the limited number of lunar observations available. Approximately 15 sunrise and 15 sunset measurements were made per day in solar occultation mode; however, due to the orbital characteristics of the Meteor-3M, these measurements were made only at high northern latitudes (45° N to 80° N) for sunset measurements and at middle southern latitudes (25° S to 60° S) for sunrise measurements. During solar occultation measurements, the FOV of SAGE III/M3M, approximately 0.5 km on the limb, was repeatedly scanned across the solar disk, covering altitudes from the cloud tops to approximately 300 km. This resulted in an effective vertical resolution of 1 km. Scientific operations of SAGE III/M3M began in February 2003 and continued through to March 2006.

SAGE III/M3M solar occultation measurements are used to retrieve number density profiles of several gases, as well as profiles of aerosol extinction, temperature, and pressure. The SAGE III/M3M ozone and $\mathrm{NO_2}$ retrieval algorithm is detailed in the SAGE III Algorithm Theoretical Basis Document (SAGE III ATBD, 2002) and Wang et al. (2006). This algorithm uses a multiple linear regression technique to determine slant-path column densities of ozone and $\mathrm{NO_2}$ simultaneously from derived

slant-path optical depth measurements. These columns are then inverted using a Chahine technique to give vertical profiles on a uniform 0.5 km grid. NO_2 is retrieved from the cloud tops to 50 km, while ozone is retrieved up to 85 km. The retrieval requires temperature and pressure information for the atmosphere, which comes from the National Oceanic and Atmospheric Administration (NOAA) National Centers for Environmental Prediction (NCEP) below 0.4 hPa, above which climatological data are used from GRAM-95 (Justus and Johnson, 1997). This information is used to convert the SAGE III/M3M number density profiles into VMR profiles. The version 4 SAGE III/M3M data products are used in this study for the period from February 2004 to December 2005.

The SAGE III/M3M data is pre-screened by the retrieval team before release, though Thomason et al. (2010) recommends additional filtering for several periods in early 2002 where poor ephemeris data affected pointing knowledge. However, since only SAGE III/M3M data coincident with MAESTRO data are used here, no additional filtering was necessary.

SAGE III/M3M version 4 ozone data has been compared previously by Davis et al. (2016) against coincident ozonesonde measurement, and agreement to within 5 % over the entire stratosphere was found. Climatological comparisons of the version 4 SAGE III/M3M ozone against a MIM climatology show agreement to within 10 % over virtually the entire stratosphere, with SAGE III/M3M yielding more ozone in the mid-stratosphere and less in the upper and lower stratosphere (SPARC-DI, 2017). Comparisons of NO_2 zonal mean profiles against MIM profiles in the SPARC-DI (2017) showed that version 4 SAGE III/M3M NO_2 is about 10 % higher than the MIM in the middle stratosphere, while differences below 20 km can exceed 30 % and those above 35 km can exceed 50 %. This is in agreement with the work of Sheese et al. (2016), who compared version 3 SAGE III/M3M NO_2 against that of ACE-FTS and found the SAGE III/M3M product to be about 10 % larger than that of ACE-FTS between about 22 and 40 km.

2.8 International Space Station

The International Space Station (ISS) has been in low-earth orbit (420 km, 51.6° inclination) since November 1998. Aboard the ISS is an array of instrument that have cycled over time, including the Stratospheric Aerosol and Gas Experiment III on the International Space Station (SAGE III/ISS), which was installed February 2017.

2.8.1 SAGE III/ISS

SAGE III/ISS is a grating spectrometer that operates from 280–1035 nm over 86 spectral channels, with an additional photodiode that measures at 1542 nm (McCormick et al., 2020; Wang et al., 2020). SAGE III/ISS makes solar and lunar occultation measurements, though only the former are considered here, with approximately 15 sunrises and 15 sunsets measured each day. Solar occultation measurements are made by scanning the approximately 0.5 km effective FOV of the instrument across the solar disk, resulting in multiple measurements at each altitude. Scientific operations of SAGE III/ISS commenced in June 2017 and continue through to the present (Dubé et al., 2021).

The solar occultation measurements from SAGE III/ISS are used to produce vertical profiles of ozone, water vapour, NO_2, aerosol extinction, temperature, and pressure. The ozone and NO_2 algorithms, detailed in the SAGE III ATBD (2002) and Wang et al. (2020), consist of determining slant-path optical depth profiles and then using a multiple linear regression technique to

determine slant-path number density profiles. This retrieved NO_2 is used to derive a second ozone product, termed the aerosol ozone (AO3) product, using a least-squares technique akin to the SAGE II retrieval. The slant-path number density profiles are converted to vertical number density profiles using a global fit inversion method. The resulting profiles are produced on a uniform 0.5 km grid, spanning from 0 to 70 km with about 1 km vertical resolution. Temperature and pressure data for the inversion come from MERRA-2, and the air density calculated from these fields is used in this study to convert the profiles from number density to VMR. In this study the version 5.3 SAGE III/ISS products are used, with the AO3 product being used for ozone, which Wang et al. (2020) showed to have the smallest biases and best precision of the SAGE III/ISS ozone products as determined from comparisons with an ensemble of satellite, ozonesonde, and Lidar measurements. The SAGE III/ISS data used in this study cover the period from July 2017 to December 2023.

Prior to release, the SAGE III/ISS products are assessed by the mission team to determine their overall quality and remove any failed retrievals (SAGE III/ISS Data Products User's Guide, 2023). Quality flags are included with the data for each retrieved profile, denoting measurements with negative or fill data in their slant-path profile, however as these flagged properties do not preclude the inversion from generating a viable number density profile, these flags have not been used to filter the data. No further filtering has been applied to the dataset.

The SAGE III/ISS version 5.1 ozone has been compared in McCormick et al. (2020) against coincident measurements from ACE-FTS, with agreement having been found to within about 5 % between 20 and 50 km and with seasonal variation as to which yielded more ozone. Similarly, Wang et al. (2020) found Aura-MLS agreed with version 5.1 SAGE III/ISS ozone to within 5 % between 18 and 50 km, with SAGE III/ISS yielding slightly more ozone overall. Comparisons against OSIRIS showed OSIRIS ozone to be about 5 % smaller over the stratosphere, while comparisons with OMPS-LP showed OMPS-LP yielded more ozone, by about 5–10 %, around 30 km, above and below which the differences increase to 20 % with SAGE III/ISS yielding more ozone (Wang et al., 2020). Comparisons by Dubé et al. (2022) showed that SAGE III/ISS version 5.2 NO_2 had larger values over most of the stratosphere by about 20 % than OSIRIS. Further comparisons performed by Strode et al. (2022) of SAGE III/ISS version 5.2 NO_2 against that of ACE-FTS showed that SAGE III/ISS agrees to within about 25 % of ACE-FTS over the stratosphere, albeit with a consistent high bias. They also found that OSIRIS NO_2 was about 50–70 % smaller than that of SAGE III/ISS below 20 km, but this difference decreased with altitude to about 10–20 % near 40 km.

3 Comparison Methodology

All the satellite measurement datasets used were interpolated onto a uniform 1 km vertical grid, spanning from 0 to 100 km, chosen to match the effective vertical resolution of the MAESTRO dataset. The datasets were linearly interpolated without the use of smoothing using instrument averaging kernels (e.g., Dupuy et al., 2009; Adams et al., 2012). As the MAESTRO version 4.5 retrievals are only weakly constrained above 80 km, this study focuses between 5 and 80 km where most of the retrieved profile information is located.

In order to compare measurements from different instrument sets, spatial and temporal coincidence criteria were employed. Following analyses by Sheese et al. (2021), who compared the effects of coincidence criteria against geophysical variability, in

this study measurements are deemed coincident if they are made within 8 hours of each other and within 1000 km. If multiple measurements from a comparison dataset are coincident with a MAESTRO profile, only the profile measurement closest in time is used for analysis; thus every MAESTRO profile is coincident with at most one profile from each other satellite dataset.

As a solar occultation instrument, MAESTRO has relatively sparse spatial and temporal sampling so when employing coincidence criteria for comparisons, as done here, the potential exists for sampling biases to impact the results. This is likely to occur when comparison instruments also provide sparse or seasonally-varying coverage, with the biases resulting from comparisons that do not wholly capture the state of the atmosphere or which result in systematic differences in sampling locations. In this study, a number of instruments with both sparse and dense sampling are employed. The latter, which includes Odin-SMR, SCIAMACHY, MIPAS, Aura-MLS, and OMPS-LP yield comparisons with minimal potential for sampling biases to impact the results of the analysis as the measurement comparisons are generally evenly distributed across space and time. ACE-FTS, while itself also a solar occultation instrument with the sparse sampling that entails, shares a line-of-sight with MAESTRO and so every measurement made by MAESTRO is coincident with one from ACE-FTS, avoiding any systematic differences in measurement locations.

In contrast, OSIRIS is a densely sampling instrument that possesses a seasonal asymmetry in its coverage, generally only covering one hemisphere at a time, while the remaining four instruments employed in this study, GOMOS and the three SAGE instruments, all provide sparse sampling. The sparse sampling of these last four instruments is due to the limitations, addressed above, of the solar occultation technique employed by the SAGE instruments, and the limited number of viable stellar occultation measurements made by the former. Thus, for OSIRIS, GOMOS, and the SAGE instruments there exists the possibility that any comparisons made with them will be affected by sampling biases. This is particularly true for SAGE II since throughout the overlap period of SAGE II with MAESTRO, SAGE II was only operating at a 50 % duty cycle, which, when combined with the orbits of ERBS and SCISAT, causes all coincident measurements to be largely confined to a few narrow groupings, often near the edges of the polar vortex where variability is high.

Despite the potential for sampling biases, this study includes these sparse sampling/seasonally asymmetric datasets for the assessment of the MAESTRO version 4.5 products to allow for an overview of the MAESTRO data in comparison to a diverse suite of measurements made using multiple techniques, with the caveat that some of these comparisons might be affected by sampling biases and should be considered as part of an ensemble of comparisons rather than independently.

Following prior work in validating satellite measurement datasets, particularly those which have assessed previous versions of the MAESTRO products (e.g., Kerzenmacher et al., 2005; Dupuy et al., 2009; Adams et al., 2012; Loew et al., 2017; Bognar et al., 2019), agreement between MAESTRO and the various other satellite datasets is assessed through a set of diagnostic metrics: namely the mean absolute difference, the mean relative difference, and the Pearson correlation coefficient. The mean absolute difference, Δ_{abs}, compares MAESTRO measurements, M, with coincident measurements from a comparison instrument, C, as in Eq. 1:

$$\Delta_{abs} = \frac{1}{N}\sum_{i=1}^{N}(M_i - C_i), \tag{1}$$

where N is the number of coincident measurements between the two instruments. The mean relative difference, Δ_{rel}, is also calculated between pairs of coincident measurements, in this case using Eq. 2:

$$\Delta_{rel} = 100\% \times \frac{1}{N} \sum_{i=1}^{N} \frac{M_i - C_i}{\frac{1}{2}(M_i + C_i)}. \quad (2)$$

In addition to the mean of these two metrics, their standard deviations were also calculated. The third main diagnostic metric used here is the Pearson correlation coefficient, r, which is calculated as in Eq. 3:

$$r = \frac{1}{N-1} \sum_{i=1}^{N} \left(\frac{M_i - \bar{M}}{\sigma_M} \right) \left(\frac{C_i - \bar{C}}{\sigma_C} \right) \quad (3)$$

where $\bar{M}$ and $\bar{C}$ are the means of the MAESTRO and comparison datasets at a given altitude, and σ_M and σ_C are their standard deviations.

When comparing measurements of NO_2, special consideration must be allowed for the strong diurnal cycle that arises due to the photolysis of NO_2 into NO throughout the daylight hours and the sharp temporal gradients observed thereof, particularly at sunrise and sunset. These require that comparisons between measurement datasets are made at approximately the same time local solar time. Solar occultation instruments, such as MAESTRO, always make measurements during the same time(s) of day, and so these datasets can be intercompared without the need for diurnal scaling, so long as sunrise measurements are compared to sunrise measurements and sunset to sunset. Other observation techniques can vary in the time of day at which they measure, and to facilitate comparisons of NO_2 observations they need to be scaled to the same time of day. Often this is accomplished through the use of a photochemical box model (e.g., Adams et al., 2012; Bognar et al., 2019; Dubé et al., 2021); however, global scaling factors can also be used to similar effect.

In this study, diurnal scaling of NO_2 is accomplished through the use of monthly multiyear-mean zonal-mean scaling factors produced by Strode et al. (2022). These climatological scaling factors are generated from four years of model output, spanning 2017–2020. The simulated ozone, NO_2 and other trace gas distributions for this are modelled with the global three-dimensional Goddard Earth Observing System (GEOS; Molod et al., 2015) model, coupled to the Global Modeling Initiative (GMI; Duncan et al., 2007; Strahan et al., 2007; Nielsen et al., 2017) stratospheric and tropospheric chemistry mechanism and the Goddard Chemistry Aerosol Radiation and Transport (GOCART; Chin et al., 2002; Colarco et al., 2010) aerosol module. The resulting scaling factors are functions of altitude, latitude, and solar zenith angle and allow for the scaling of NO_2 concentrations to local sunrise and/or sunset. These scaling factors have been applied to scale all coincident measurements from the non-solar-occultation instruments used in this study. While it is possible to compare the three SAGE instruments to MAESTRO without the use of diurnal scaling, so long as local sunrise measurements are compared to local sunrise measurements and local sunset to local sunset, this limits the number of potential coincidences that can be examined due to differences in the orbits of these instruments and the short overlap period between MAESTRO and that of SAGE II and SAGE III/M3M. To maximize the number of comparisons with the SAGE instruments, rather than force sunrise-sunrise and sunset-sunset comparisons, the diurnal scaling factors from Strode et al. (2022) have been employed.

Ozone has also been shown to experience a diurnal cycle (Prather, 1981, e.g.,). During the day, molecular oxygen is photolyzed to produce odd oxygen (O_x = O + O_3) species which then undergo subsequent reactions. Due to the influence of

pressure on these reactions, odd oxygen is preferentially converted into ozone in the stratosphere during the day; however, at higher altitudes, more odd oxygen is stored as atomic oxygen during the day. Thus, the concentration of stratospheric ozone peaks in the afternoon, and that of the mesosphere peaks in the night when all atomic oxygen recombines. This diurnal cycle is largest in the upper stratosphere and mesosphere, but still exceeds 2 % in the middle stratosphere (Prather, 1981; Sakazaki et al., 2013). Combined with the effects of vertical transport by atmospheric tidal winds, this leads to a distinct difference in observed ozone values between sunrise and sunset measurements for solar occultation instruments (e.g., Sakazaki et al., 2013, 2015; Wang et al., 2020). This difference between the sunrise and sunset measurement values, and the resulting bias between the two, has been noted in previous MAESTRO validation efforts (Kar et al., 2007). To minimize the effects of this difference between the two types of measurements, the MAESTRO sunset and sunrise measurements are treated independently for the calculation of the above metrics in this study. Additionally, diurnal scaling factors for ozone from Strode et al. (2022) have been applied at all altitudes to all comparison datasets, except for ACE-FTS, as done for NO_2.

4 Results

The results are presented for the Vis.-ozone product in Sect. 4.1, for UV-ozone in Sect. 4.2, and for NO_2 in Sect. 4.3. For clarity, the set of profiles constructed from the measurements from the comparison instruments that are coincident with MAESTRO sunrise (sunset) measurements are referred to in the following section as the sunrise (sunset) profiles, or the sunrise (sunset) coincident profiles, of the comparison instruments. The discussion of each MAESTRO product is divided into two subsections: one addressing the overall mean profiles from MAESTRO and the comparison instruments, and one addressing comparison metrics.

4.1 Vis.-ozone

Comparisons between MAESTRO sunrise and sunset Vis.-ozone data against diurnally-scaled (where required) coincident measurements are shown in Figs. 1 through 4.

4.1.1 Profile overview

Figure 1 shows the mean MAESTRO sunrise and sunset profiles, along with the mean of all profiles from the comparison instruments coincident with either the sunrise or sunset MAESTRO profiles separated accordingly. The standard deviation of these are shown alongside the mean profiles, and the number of coincident measurement pairs found for the MAESTRO sunrise/sunset measurements are shown below the names of each comparison dataset.

Generally, the MAESTRO mean ozone profiles are found to peak between 30 and 40 km, in broad agreement with the comparison datasets, with a sharp drop off above 50 km that shows a faster decrease in ozone concentration with altitude than observed for most of the comparison datasets. Near the ozone peak, the MAESTRO mean profiles tend to be slightly high biased, as compared to the coincident datasets, with the largest biases found in comparisons made with Odin-SMR, GOMOS, SAGE II, and sunset-coincident SAGE III/ISS measurements. Above about 50 km, the sharp decrease in MAESTRO ozone

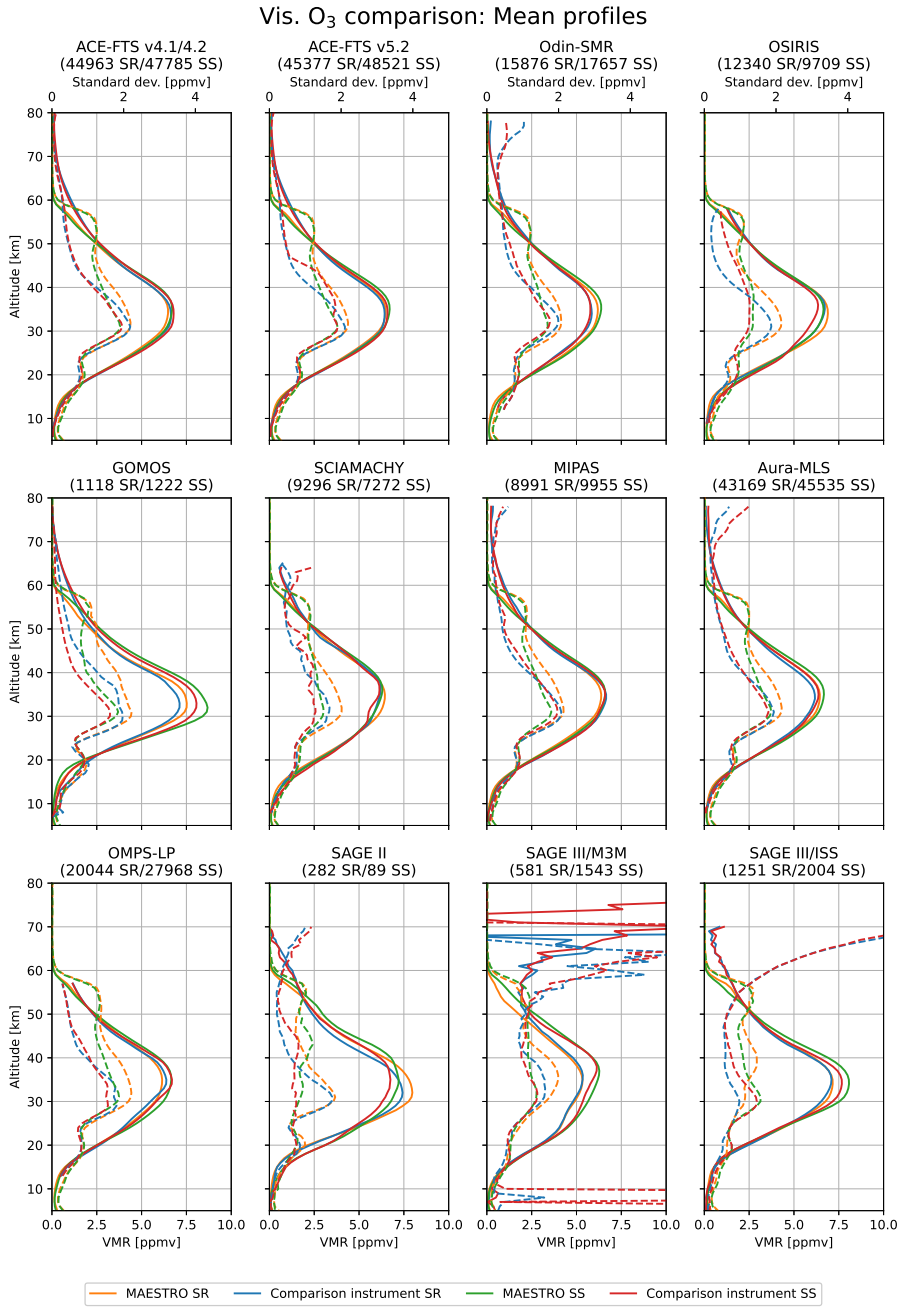

Figure 1. Comparison of the mean MAESTRO sunrise (SR) and sunset (SS) Vis.-ozone profiles with mean coincident ozone profiles from the comparison instruments outlined in Sect. 2. The profiles from the comparison instruments are divided into whether they are coincident with MAESTRO sunrise or sunset measurements. The mean profiles are presented using the lower x-axis scale. The 1σ standard deviations of the profiles are shown as dashed lines using the upper x-axis scale. Under each instrument name is the number of coincident measurement pairs found for the MAESTRO sunrise/sunset measurements.

leads to a distinct low bias compared to the other datasets that extends to the top of the profiles. The standard deviation of the MAESTRO profiles peaks about 5 km below the mean stratospheric ozone maximum and general agreement is found in the shape and magnitude of these profiles with those from the coincident datasets up to about 35 km. Above this altitude, between approximately 40 and 55 km, the MAESTRO standard deviation profiles are near 2.5 ppmv, whereas over this range most of the coincident standard deviation profiles are less than half of that. Between about 60 and 80 km, the standard deviation profiles of MAESTRO are near 0 ppmv, an underestimation of the standard deviation compared to most of the other instruments. Finally, for most of the mean profile sets, with exception for the OSIRIS, SCIAMACHY, and SAGE II profiles, the sunset profiles tend to be somewhat larger than the sunrise data. This is particularly evident in the comparisons with the GOMOS, SAGE III/M3M and SAGE III/ISS instruments. In contrast, for the standard deviation profile sets, the sunrise profiles are found to be generally larger than the sunset profiles. This supports the separation of the comparisons into sunrise and sunset subsets.

Good agreement is found between between MAESTRO and both the ACE-FTS version 4.1/4.2 and version 5.2 datasets from the troposphere to 50 km. Above this altitude, the MAESTRO and ACE-FTS profiles diverge, with the MAESTRO profiles yielding lower ozone up to the top of the profile. With exception for the ACE-FTS v5.2 sunset profiles, the MAESTRO standard deviation is found to be larger than that of ACE-FTS between 30 and 60 km. The largest differences in these standard deviation profiles occur around 55 km, where the ACE-FTS v5.2 sunset profile also are found to fall to lower values than the corresponding MAESTRO profile. Above 60 km, the near 0 ppmv MAESTRO standard deviation profiles are smaller than those profiles from ACE-FTS. Minimal differences are observed between comparisons made against the two versions of ACE-FTS. The comparisons with MIPAS are largely similar to those with ACE-FTS, with the two mean MIPAS ozone profiles overlapping significantly with each other and with the two mean MAESTRO ozone profiles below 50 km, and with similar standard deviation profiles as observed with ACE-FTS. However, above 65 km, the MIPAS standard deviation profiles are found to be significantly larger than those observed for ACE-FTS or MAESTRO.

Generally good agreement is found with the SCIAMACHY, Aura-MLS, and OMPS-LP comparisons; however, only Aura-MLS reaches to the top of the MAESTRO profile, so the other two cannot be used to assess the representation of mesospheric ozone from MAESTRO. The profiles from Aura-MLS differ from those from MAESTRO by about 0.5 ppmv in the middle stratosphere; however, a more pronounced difference is visible between the mean sunrise and sunset coincident profiles, which are found to differ from each other to a greater extent than for the previously discussed datasets. In the mesosphere, the Aura-MLS comparisons are found to be similar to those made with MIPAS, with larger ozone standard deviation and slightly larger mean ozone values over this range than observed with ACE-FTS and MAESTRO. For the comparisons with SCIAMACHY, the largest differences in the mean ozone profiles are found just below the stratospheric ozone maximum, where MAESTRO is found to yield larger ozone VMRs by about 0.5 ppmv. Other than that, the two datasets are found to broadly agree between approximately 15 and 55 km. Lastly, the coincident OMPS-LP profiles are found to yield smaller mean VMRs than MAESTRO between 25 and 33 km and similar to slightly larger mean VMRs between 33 and 40 km, but overall good agreement is found through most of the profile, similar to that observed for the previous two datasets. Notable across the six sets of comparisons discussed so far is that the comparison datasets are from those least likely to be affected by sampling biases, due to the density

of their sampling or their shared line-of-sight with MAESTRO, reinforcing the good agreement found with the MAESTRO Vis.-ozone product.

From about 15 to 50 km, SAGE III/M3M is found to be in generally good agreement with MAESTRO; however, there is a large difference of about 1 ppmv observed between the sunrise and sunset sets of profiles that exceeds the differences observed for the aforementioned datasets. In the lower and middle stratosphere it is expected that the sunrise and sunset profiles should generally agree with each other due to the small diurnal cycle of ozone at these altitudes. Thus the observed difference between the sunset and sunrise profiles is likely influenced by some form of sampling bias associated with the sparse coverage and few coincidences found between MAESTRO and SAGE III/M3M. Outside of the stratosphere, the SAGE III/M3M profiles are found to be highly variable, with large oscillations in the mean SAGE III/M3M profiles below 10 km and above 60 km, which are accompanied by large jumps in the SAGE III/M3M standard deviation profiles and exponential growth in these profiles at high altitudes. These features are not reflected in the MAESTRO, or other comparison, datasets.

Somewhat similar agreement is found with Odin-SMR and OSIRIS, with both comparison datasets yielding less ozone than MAESTRO near the stratospheric ozone maximum. Around this maximum, the comparison profiles are typically within about 0.5 ppmv of those from MAESTRO. However, in the comparisons made with OSIRIS, there is an additional difference of about 0.5 ppmv near this peak between the sunrise and sunset profiles, with the sunrise measurement profiles yielding the larger concentrations. As with the SAGE III/M3M comparisons, this indicates the potential for sampling bias to play a role in the OSIRIS comparisons; however, given the greater degree of agreement between the sunrise and sunset profiles observed here as compared to those for the SAGE III/M3M comparisons, it is likely that it is a more limited effect. Further from the ozone peak, good agreement is found with MAESTRO and these two datasets, with the comparisons made with OSIRIS yielding the better agreement below 25 km and above 40 km. Above 60 km, the Odin-SMR mean and standard deviation profiles are similar to those from MIPAS and Aura-MLS, which reinforces the underestimation of ozone and ozone variability by MAESTRO above the stratosphere. The OSIRIS profiles do not extend up to 80 km, so they cannot be used to assess the agreement of mesospheric ozone.

The remaining datasets all show larger differences from MAESTRO, as well as generally larger differences between their sunset and sunrise profiles that potentially arise from sampling biases. Beginning with GOMOS, comparisons with MAESTRO indicated that the latter has larger ozone values than the former, often in excess of 0.5 ppmv between 20 and 50 km, with the four profiles spread apart by approximately 2.5 ppmv. Between 60 and 70 km the GOMOS profiles have larger ozone concentrations than MAESTRO, by up to about 1.2 ppmv, in closer agreement to what was observed for many of the prior comparisons. Despite the disagreement in much of the magnitude of the mean profiles, the GOMOS comparisons share many profile features with those comparisons already touched upon. A similar spread in profiles is observed with the SAGE III/ISS comparisons, albeit with a maximum spread of only 1.5 ppmv, as opposed to 2.5 ppmv, near 35 km. As with GOMOS, SAGE III/ISS is found to have better agreement with MAESTRO for sunrise measurements than sunset measurements, with the pair of mean sunset profiles also having been found to have larger maximum ozone VMRs. The SAGE III/ISS standard deviation profiles are found to increase exponentially above 55 km, reaching the largest values of any of the measurement datasets

assessed. Only the SAGE III/M3M standard deviation profiles are found to yield similar exponential growth in their standard deviation profiles at these high altitudes.

Lastly, significant disagreement is observed with the SAGE II comparisons, which possess features in their mean comparison profiles not seen with the other comparisons. The source of this disagreement is likely due to the limited number of comparisons that were possible between the SAGE II and MAESTRO datasets. These two datasets had the shortest overlap period, and only 371 comparisons could be made for the Vis.-ozone product, nearly an order of magnitude fewer comparisons than for the dataset with the next fewest coincident measurements. Thus the agreement, or lack thereof, between MAESTRO and SAGE II should be treated with a degree of caution. Addressing the comparisons it is found that the MAESTRO Vis.-ozone product is larger than that from SAGE II between 20 and 50 km by as much as 0.8 ppmv. Additionally, the sunrise coincident profiles are found to possess larger ozone concentrations than the sunset profiles by about 1 ppmv in the middle stratosphere. Unlike other datasets, the ozone peak occurs at a lower altitude for the sunrise comparisons than the sunset comparisons. The SAGE II sunset standard deviation profiles are found to remain around 1 ppmv from 20 to 45 km, dropping to near half of this around 55 km, and finally increasing to 1 ppmv above 60 km alongside the SAGE II sunrise standard deviation profile. This last increase is found to be similar to what is observed for the sunset SCIAMACHY profiles.

4.1.2 Comparison metrics

Having addressed the general profile properties from each dataset, focus can turn to the comparison metrics outlined in Sect. 3. Figures 2 and 3 show the absolute and relative differences between the MAESTRO sunrise and sunset measurements and those measurements coincident with these from the other twelve datasets. From these comparisons, it is found that MAESTRO Vis.-ozone shows generally good agreement with the comparison datasets between approximately 20 and 50 km, with generally similar agreement for both the sunrise and sunset measurements. These comparisons indicate that MAESTRO Vis.-ozone is generally biased high between 20 and 50 km, with the only comparisons consistently indicating otherwise being those made with ACE-FTS version 4.1/4.2 and with the MIPAS sunrise coincident measurements. Between 50 and 80 km, a low bias is found for the MAESTRO data as the MAESTRO concentrations fall to near 0 ppmv by about 55 km. Taken with the extremely low standard deviation for MAESTRO over this range, this suggests that the MAESTRO retrieval may be over-constrained in the mesosphere, leading to the partitioning of ozone into the stratosphere and contributing to the high bias observed there. Below 20 km, the profile comparisons show small absolute differences, but large relative differences with high variability, rendering comparisons over this span spurious, especially when coupled to the high uncertainty many of the comparison datasets have at low altitudes.

Focusing between 20 and 50 km, where the overall closest agreement is observed, MAESTRO measurements agree best with ACE-FTS version 4.1/4.2, ACE-FTS version 5.2, and MIPAS, which have averaged absolute differences over this vertical range for sunrise (sunset) measurements of 0.11 (0.11) ppmv, 0.10 (0.12) ppmv, and 0.12 (0.13) ppmv respectively. This profile-averaged metric was calculated using the unsigned magnitude of the differences to avoid oppositely signed values from cancelling. These differences translate into profile-averaged relative differences of 4.8 (3.1) % for ACE-FTS version 4.1/4.2, 2.5 (2.5) % for ACE-FTS version 5.2, and 3.3 (2.8) % for MIPAS over this range. Very good agreement is also found with

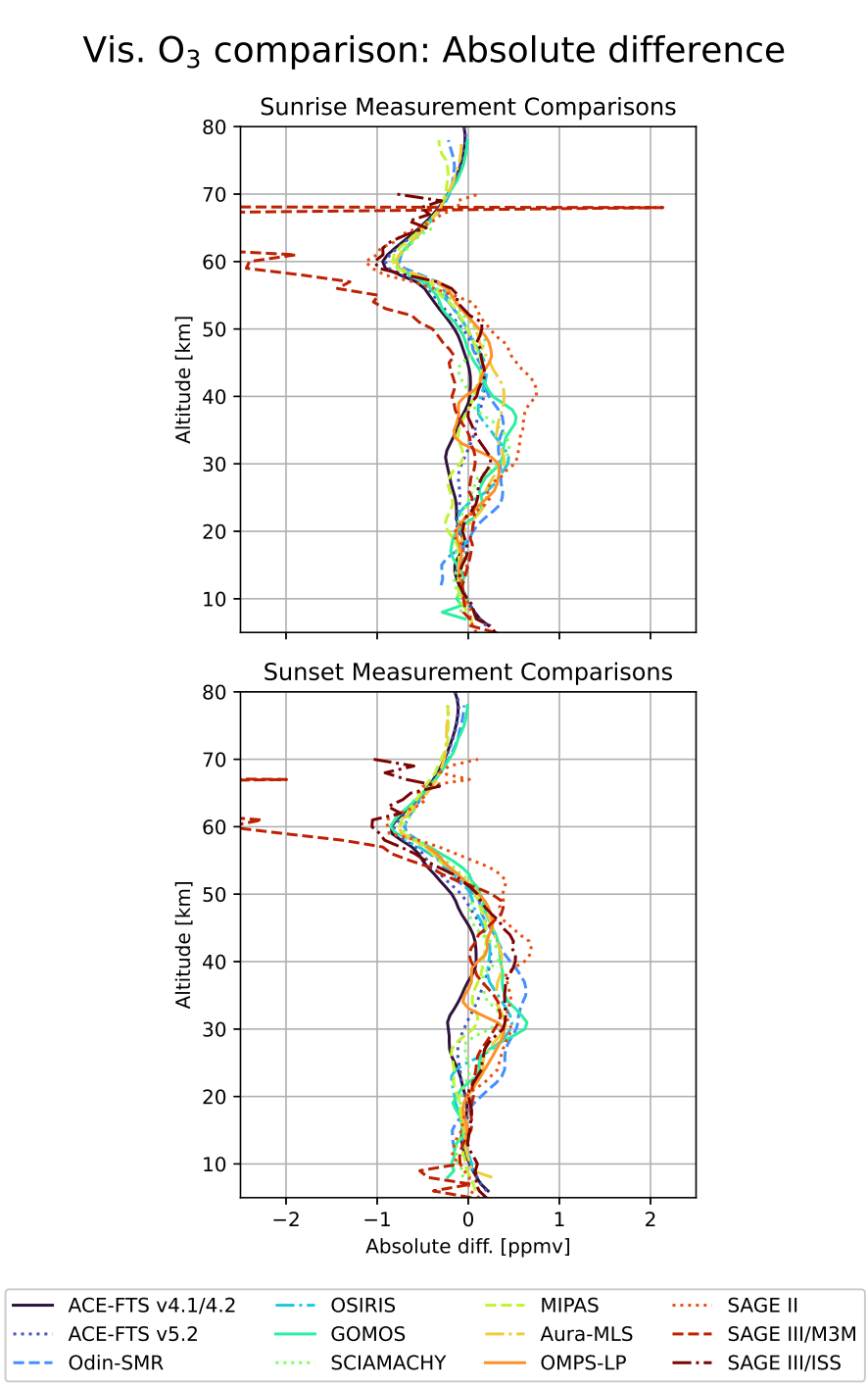

Figure 2. Mean absolute difference between MAESTRO sunrise (top) and sunset (bottom) Vis.-ozone measurements and coincident ozone profiles from the comparison instruments outlined in Sect. 2.

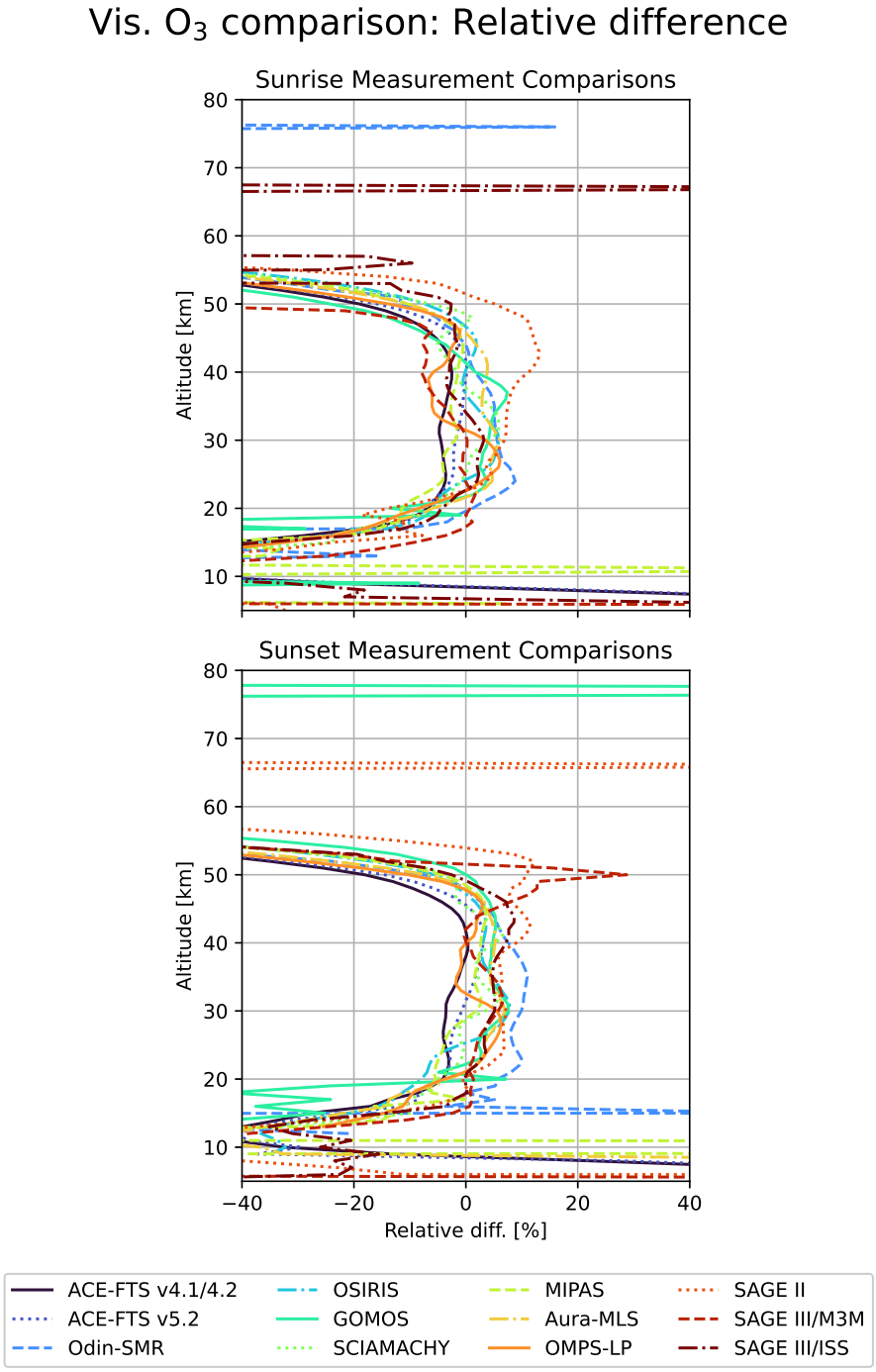

Figure 3. Same as Fig. 2 but for the relative difference.

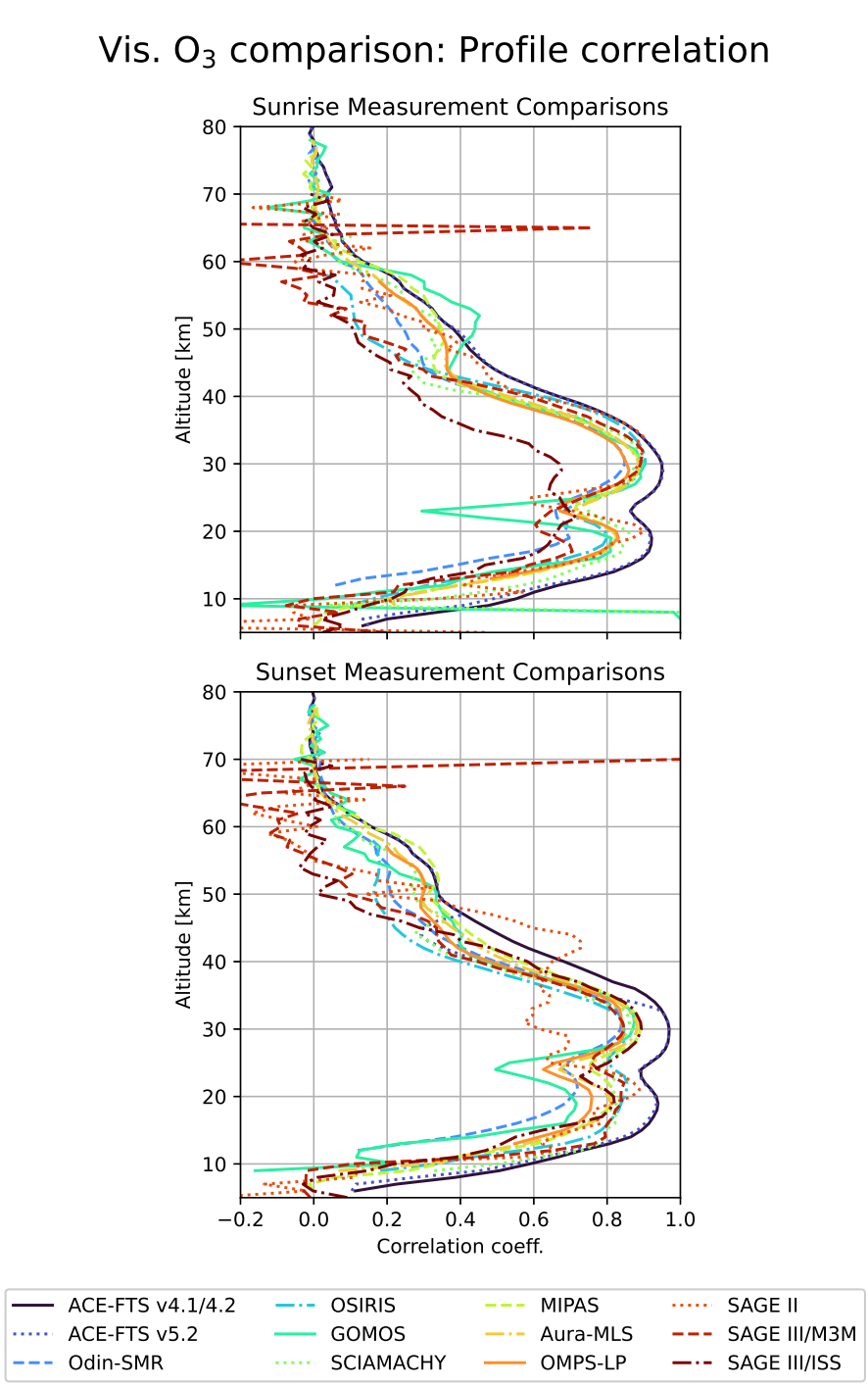

Figure 4. Pearson correlation coefficient between the MAESTRO sunrise (top) and sunset (bottom) Vis.-ozone measurements and coincident ozone profiles from the comparison instruments outlined in Sect. 2.

Table 2. Mean unsigned absolute (Δ_{abs}) and relative (Δ_{rel}) differences calculated between MAESTRO Vis.-ozone sunrise (sunset) measurements and coincident measurements from the comparison datasets shown in the first column, averaged over three altitude ranges (Alt. range) covering 15–20 km, 20–50 km, and 50–80 km. This profile-averaged metric was calculated using the unsigned magnitude of the differences to avoid oppositely signed values canceling.

Alt. range	15–20 km		20–50 km		50–80 km	
Metric	Mean Δ_{abs} (ppmv)	Mean Δ_{rel} (%)	Mean Δ_{abs} (ppmv)	Mean Δ_{rel} (%)	Mean Δ_{abs} (ppmv)	Mean Δ_{rel} (%)
ACE-FTS v4.1/4.2	0.09 (0.03)	22.0 (14.6)	0.11 (0.11)	4.8 (3.1)	0.38 (0.40)	144.9 (148.4)
ACE-FTS v5.2	0.08 (0.02)	19.7 (11.2)	0.10 (0.12)	2.5 (2.5)	0.35 (0.37)	153.1 (147.5)
Odin-SMR	0.14 (0.09)	140.1 (14.3)	0.25 (0.40)	4.4 (7.6)	0.32 (0.31)	141.3 (143.9)
OSIRIS	0.05 (0.09)	17.7 (14.1)	0.19 (0.24)	2.7 (4.4)	0.26 (0.28)	40.2 (45.5)
GOMOS	0.17 (0.11)	74.3 (30.7)	0.23 (0.31)	5.3 (4.5)	0.33 (0.31)	144.7 (140.3)
MIPAS	0.12 (0.07)	21.9 (8.3)	0.12 (0.13)	3.3 (2.8)	0.37 (0.36)	138.5 (141.2)
SCIAMACHY	0.11 (0.07)	17.7 (9.0)	0.16 (0.14)	3.0 (2.7)	0.41 (0.39)	101.6 (95.1)
OMPS-LP	0.09 (0.04)	20.1 (10.5)	0.17 (0.17)	4.3 (2.6)	0.14 (0.20)	46.0 (50.7)
Aura-MLS	0.08 (0.05)	20.4 (13.3)	0.26 (0.26)	3.7 (4.2)	0.30 (0.35)	141.9 (149.6)
SAGE II	0.06 (0.04)	14.7 (4.8)	0.45 (0.41)	8.2 (7.1)	0.47 (0.43)	116.7 (111.5)
SAGE III/M3M	0.02 (0.03)	2.9 (1.2)	0.11 (0.18)	4.5 (4.0)	4.67 (6.95)	147.8 (136.2)
SAGE III/ISS	0.03 (0.03)	16.1 (4.0)	0.11 (0.31)	2.3 (4.7)	0.49 (0.62)	177.8 (124.7)

OSIRIS, SCIAMACHY, OMPS-LP, SAGE III/M3M, and sunrise measurements from SAGE III/ISS. Comparisons with Odin-SMR and SAGE II show the poorest agreement over this range, with average absolute differences of 0.25 (0.40) ppmv and 0.45 (0.41) ppmv respectively for sunrise (sunset) comparisons, however these translate into average relative differences of 4.4 (7.6) % for Odin-SMR, and 8.2 (7.1) % for SAGE II, indicative that the MAESTRO Vis.-ozone product is still generally in good agreement in the range of 20 to 50 km. Despite this, the agreement with SAGE II should still be treated with a degree of caution due to the extremely limited number of comparisons that were possible with the two datasets.

Between 15 and 20 km, near the lower bounds of many of the instrument measurements, most of the datasets continue to show reasonable agreement with MAESTRO, with most of the sunrise (sunset) MAESTRO measurements agreeing with the comparison datasets to within 22.0 (14.6) %. The main exceptions to this are the comparisons with the GOMOS instrument, which show values differing by 74.3 (30.7) % on average for sunrise (sunset) comparisons, and the sunrise Odin-SMR comparisons which show a 140.1 % difference on average. Below this altitude range, the comparisons show significant disagreement, often displaying differences at particular altitudes in excess of 50 %. Similarly, above 50 km, the comparisons generally show considerable disagreement, with differences reaching over 100 %.

These results indicate that there is excellent agreement between MAESTRO and the other datasets between 20 and 50 km, and good agreement from 15 to 20 km, but poor agreement in the troposphere and mesosphere. The absolute and relative

differences are summarized in Table 2 for three altitude regimes, corresponding to 15–20 km, where generally fair agreement is found, 20–50 km, where excellent agreement is found, and 50–80 km, where poor agreement is found.

Lastly, the correlation between the MAESTRO and comparison datasets is shown in Fig. 4. Here we define good correlation as having a correlation coefficient greater than 0.7, and moderate correlation as having a coefficient between 0.5 and 0.7. Across the twelve datasets, the highest correlation is observed between 15 and 40 km, where, with exception for SAGE II sunset coincident measurements and SAGE III/ISS sunrise coincident measurements, the datasets have profile-averaged correlations with MAESTRO of at least 0.71. Outside of this range, the profile correlation coefficients fall to 0.5 between 10 and 15 km and between 40 and 45 km. At 50 km, most of the correlation coefficients are between 0.2 and 0.4, with exception for SAGE III/M3M, SAGE III/ISS, and OSIRIS which are less than 0.2. As many of the comparison datasets can have spurious results near the troposphere, physical interpretations of the correlation coefficients at low altitudes are difficult. However, the drop in correlation coefficients at and above 50 km indicates that the MAESTRO Vis.-ozone product should only be used for scientific applications below this altitude, as found from the profile difference comparisons. The low correlation at high altitudes, coupled to the poor agreement at high altitudes, provides evidence that the extremely low ozone at high altitudes is likely due to a retrieval artifact as this feature is not seen in the other datasets.

4.2 UV-ozone

The comparisons between the MAESTRO sunrise and sunset UV-ozone data and the diurnally-scaled (where required) coincident ozone measurements are shown in Figs. 5 through 8. Due to the limited period of viable MAESTRO UV-ozone measurements, from the start of the mission until December 2009, there are significantly fewer coincident measurements for this set of comparisons than for the Vis.-ozone comparisons. Additionally, both OMPS-LP and SAGE III/ISS began operations after the cutoff date for the MAESTRO UV-ozone product, and so no coincidences are found with these two datasets. Finally, a comparison of the MAESTRO Vis.-ozone and UV-ozone profiles are shown in Fig. 9.

4.2.1 Profile overview

Despite a more limited number of coincident profiles, the mean MAESTRO UV-ozone profiles, comparison profiles, and standard deviations profiles, all shown in Fig. 5, are extremely similar between 20 and 50 km to those for the Vis.-ozone comparisons shown in Fig. 1. This similarity includes the small high bias previously observed for the MAESTRO dataset. Two main differences distinguish the sets of UV-ozone and Vis.-ozone profiles. The first difference is found in the mean MAESTRO profiles near 50 km, where a much sharper decrease in ozone concentration is noted for the UV-ozone product than for the Vis.-ozone product, with the VMR of ozone falling to near 0 ppmv by 55 km. The other main difference between the two products, as shown in Fig. 1 and Fig. 5, is the MAESTRO standard deviation between 30 and 60 km. In the Vis.-ozone product, the standard deviation profiles across this range generally peak around 2 ppmv at 30 km, decrease to around 1.3 ppmv between 40–45 km, and remain constant up to about 55 km before decreasing to near 0 ppmv at 60 km. In contrast, for the UV-ozone profile, the MAESTRO sunrise standard deviation profiles increase in magnitude from the troposphere up to 30 km, remain generally constant, near 2 ppmv, between 30 and 50 km, and finally decrease sharply to near 0 ppmv around 55 km. The sunset

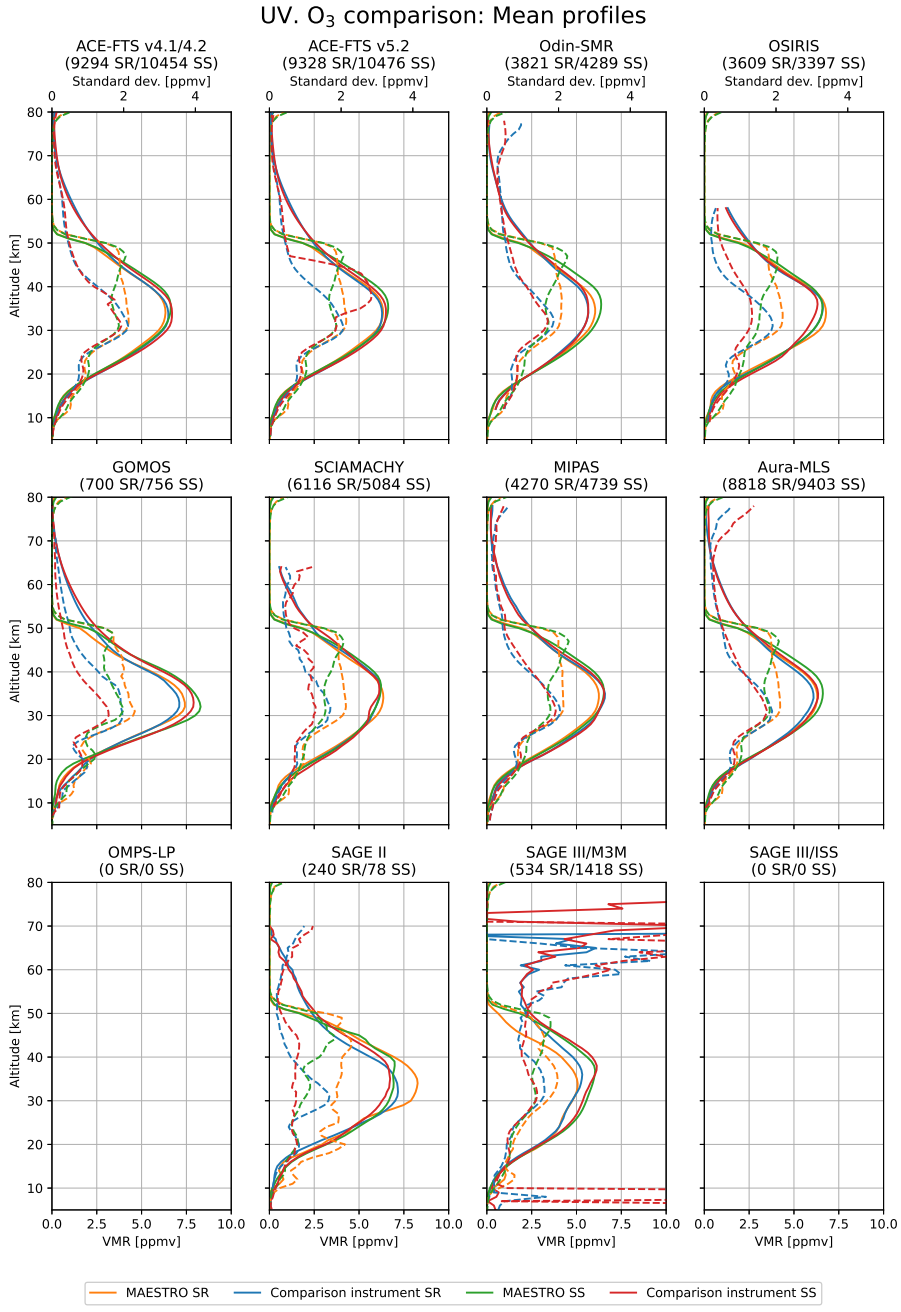

Figure 5. Same as Fig. 1 but for MAESTRO UV-ozone measurements. Note that there are no coincident measurements between the MAESTRO UV-ozone product and OMPS-LP and SAGE III/ISS.

profiles share the same increasing and decreasing behavior as the sunrise profiles below 30 km and above 50 km respectively, but the standard deviation profiles are found to peak near 45 km. Both sets of profiles indicate that despite similar profiles, the UV product is more variable than the Vis.-ozone product over much of the stratosphere.

As with the Vis.-ozone product, the UV-ozone product also underestimates the variability in the mesosphere as compared to the comparison datasets. The observed low variability in the mesosphere, coupled to the small mean VMRs in the region, can be interpreted as the result of the ozone retrieval being over-constrained to small VMR values over this span, as suggested for the Vis.-ozone product. This then can cause the retrieval to partition ozone, whose existence is derived from the optical depth spectra, into less constrained retrieval levels. The high variability observed for MAESTRO in the stratosphere provides evidence that the MAESTRO retrieval is far less constrained in this region, which allows for ozone to be readily partitioned into the stratosphere by the retrieval. This in turn might be the cause of the small high bias observed for the MAESTRO UV-ozone product. However, given the agreement between the datasets, it is likely that this has only a minor effect on the stratospheric ozone concentrations, allowing for the conclusion that the UV-ozone product is generally well-constrained only below about 50 km and should be used cautiously above this point.

4.2.2 Comparison metrics

Having addressed the main differences in the mean and standard deviation profiles from those discussed in Sect. 4.1, attention can turn to the direct comparisons between dataset pairs. As with the Vis.-ozone product, the MAESTRO UV-ozone absolute and relative differences, shown in Figs. 6 and 7 respectively, show the best agreement in the stratosphere, with MAESTRO yielding generally higher ozone concentrations than the comparison instruments. Examining the relative difference plots, it is clear that the vertical range for which good agreement is found is somewhat narrower for the UV product than the Vis.-ozone product, with the closest agreement between the datasets found between approximately 20 and 45 km. Within this range, the best agreement is found with ACE-FTS, with version 4.1/4.2 differing by 0.15 (0.19) ppmv and version 5.2 differing by 0.12 (0.20) ppmv, with GOMOS, with differences of 0.17 (0.16) ppmv, and with SCIAMACHY, with differences of 0.17 (0.16) ppmv, on average from sunrise (sunset) coincident profiles. The relative differences also reflect this good agreement, with average sunrise (sunset) differences of 5.7 (4.2) % for ACE-FTS version 4.1/4.2, 3.6 (4.0) % for ACE-FTS version 5.2, 4.8 (3.3) % for GOMOS, and 5.0 (2.8) % for SCIAMACHY. Due to greater differences near the stratospheric ozone maximum, Aura-MLS is found to have a smaller average relative difference than most of these comparisons, of 2.8 (4.2) % during sunrise (sunset), while also having larger average absolute differences, of 0.21 (0.25) ppmv. This mixed behavior emphasizes the need to include both difference metrics in this analysis.

Considering all of the datasets within the 20 to 45 km range, the majority of the comparisons have average absolute differences between 0.12 and 0.30 ppmv for the sunrise comparisons and between 0.16 and 0.34 ppmv for the sunset comparisons. The exceptions to this are the sunrise SAGE II comparisons which have an average absolute difference of 0.83 ppmv, and the sunset Odin-SMR comparisons with an average difference of 0.49 ppmv. These two datasets also show the highest relative differences, of 11.9 % and 7.6 % on average; however, these average differences indicate still reasonable agreement. The other datasets show span-averaged relative differences between 2.8 and 10.8 % for sunrise comparisons, and between 2.8 and 5.2 %

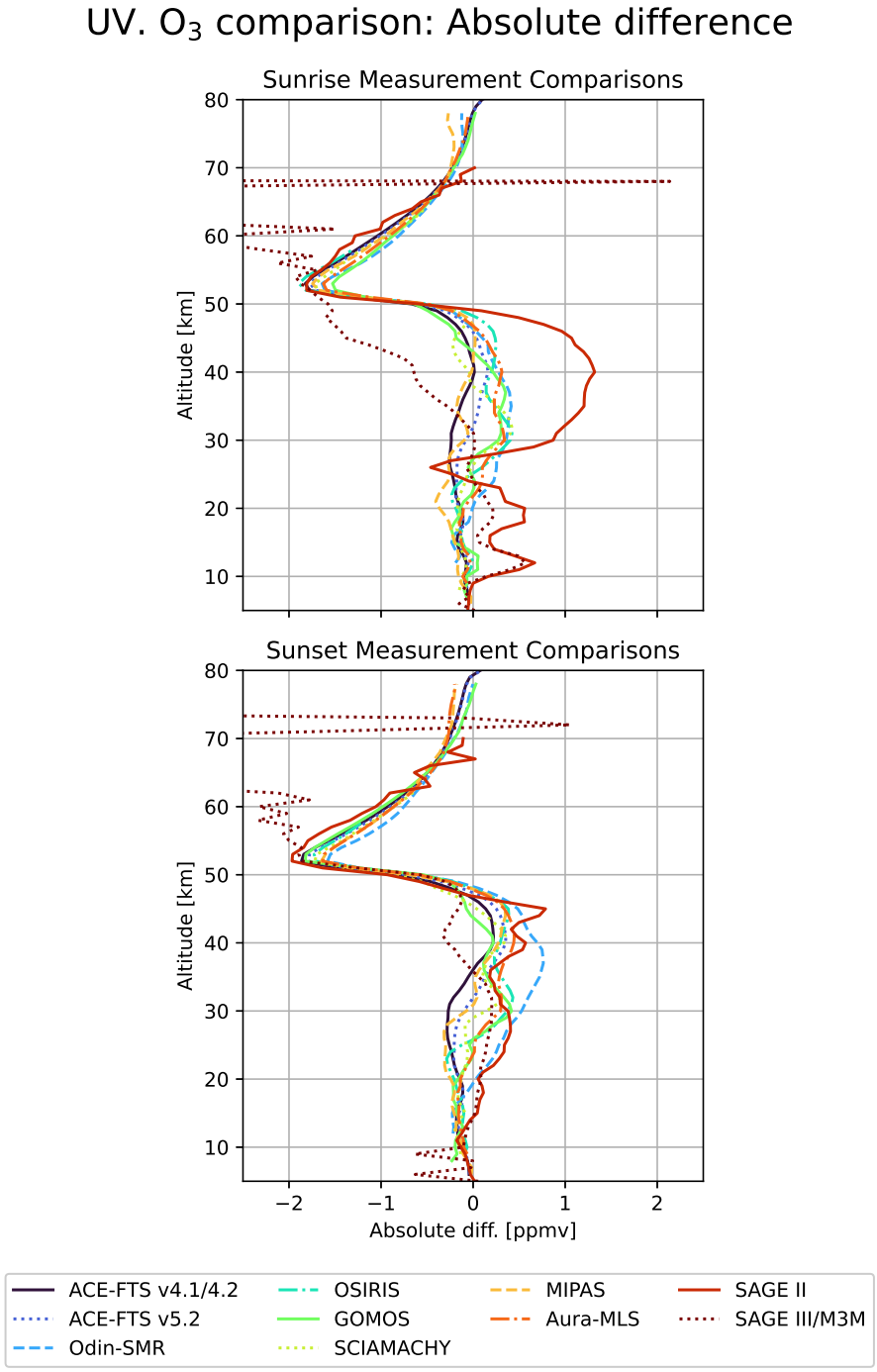

Figure 6. Same as Fig. 2 but for MAESTRO UV-ozone measurements.

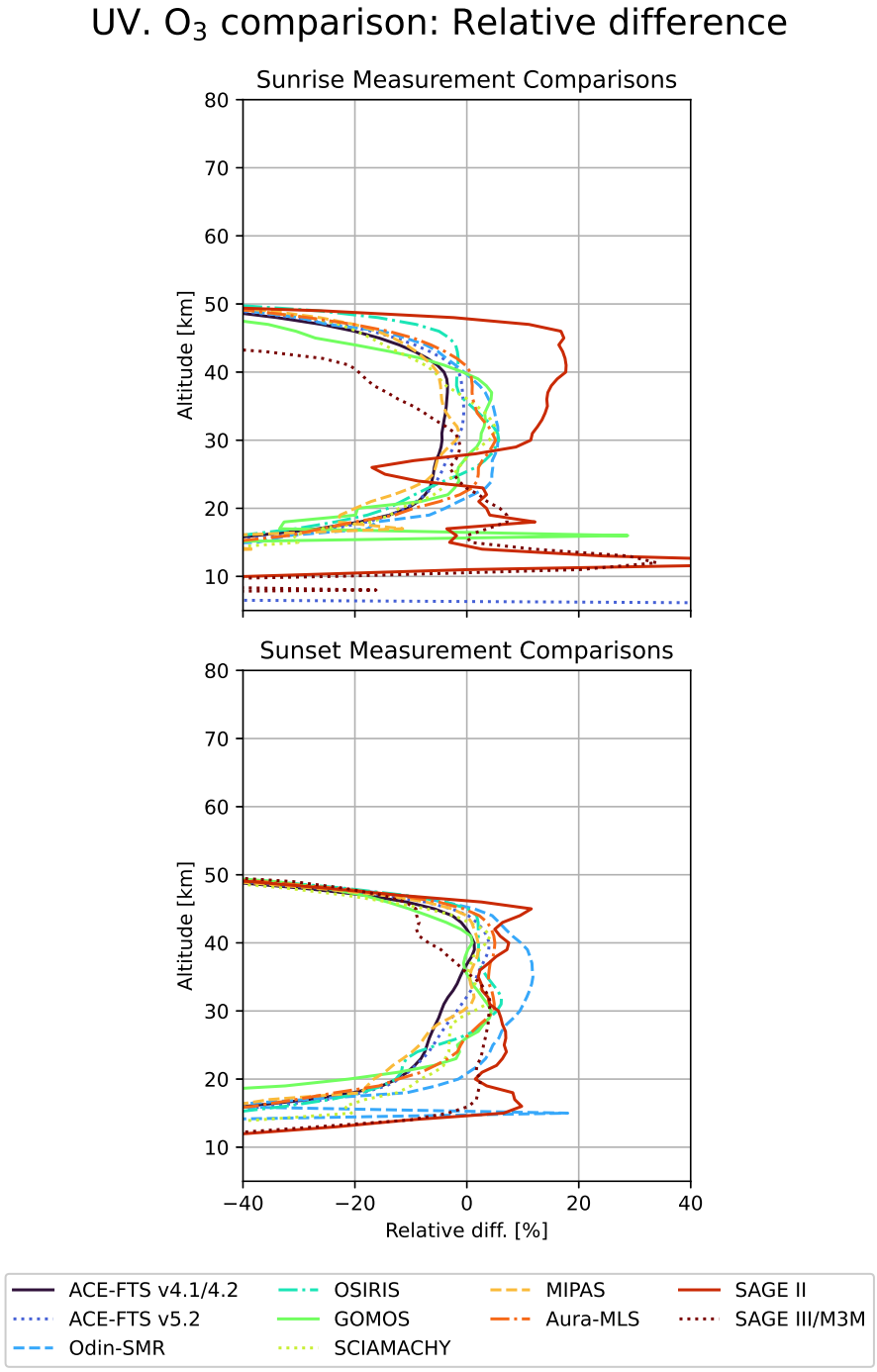

Figure 7. Same as Fig. 3 but for MAESTRO UV-ozone measurements.

Table 3. Same as Table 2 but for MAESTRO UV-ozone.

Alt. range	15–20 km		20–45 km		45–80 km	
Metric	Mean Δ_{abs} (ppmv)	Mean Δ_{rel} (%)	Mean Δ_{abs} (ppmv)	Mean Δ_{rel} (%)	Mean Δ_{abs} (ppmv)	Mean Δ_{rel} (%)
ACE-FTS v4.1/4.2	0.14 (0.14)	29.4 (31.2)	0.15 (0.19)	5.7 (4.2)	0.64 (0.64)	162.6 (159.1)
ACE-FTS v5.2	0.13 (0.12)	26.8 (28.5)	0.12 (0.20)	3.6 (4.0)	0.60 (0.61)	158.6 (158.0)
Odin-SMR	0.13 (0.13)	22.0 (21.9)	0.27 (0.49)	4.0 (7.6)	0.55 (0.55)	158.9 (159.8)
OSIRIS	0.13 (0.14)	32.6 (26.8)	0.23 (0.28)	3.9 (4.8)	1.00 (0.95)	108.0 (110.6)
GOMOS	0.20 (0.20)	33.4 (63.7)	0.17 (0.16)	4.8 (3.3)	0.58 (0.62)	160.0 (154.1)
MIPAS	0.25 (0.21)	31.2 (31.8)	0.17 (0.21)	6.6 (4.6)	0.63 (0.63)	162.4 (161.0)
SCIAMACHY	0.15 (0.14)	23.6 (16.6)	0.17 (0.16)	5.0 (2.8)	0.88 (0.90)	140.5 (141.3)
Aura-MLS	0.13 (0.16)	26.7 (31.9)	0.21 (0.25)	2.8 (4.2)	0.58 (0.62)	162.2 (164.7)
SAGE II	0.36 (0.08)	5.0 (7.3)	0.83 (0.34)	11.9 (5.2)	0.95 (0.91)	153.8 (153.3)
SAGE III/M3M	0.13 (0.04)	3.7 (1.9)	0.30 (0.17)	10.8 (4.0)	4.35 (5.42)	174.9 (162.3)

for sunset comparisons, showing that many of the datasets are in excellent agreement with MAESTRO UV-ozone in the stratosphere. As with the Vis.-ozone product, the fewest coincident measurements for the UV-ozone product are found with SAGE II, with only 318 coincident profiles found overall. Thus the comparisons with SAGE II should continue to be treated with a degree of caution.

In the lower stratosphere, between 15 and 20 km, the MAESTRO UV-ozone comparisons show larger relative differences, with the average difference of most of the datasets falling between 5.0 and 33.0 %. The best mean agreement is noted for comparisons with SAGE II and SAGE III/M3M measurements, which have a relative difference of 5.0 (7.3) % and 3.7 (1.9) % during sunrise (sunset) respectively. The GOMOS sunset coincident measurements show the largest average relative difference of 63.7 %. Even with exception for this last set of comparisons, generally poor agreement can be found in this altitude range with the majority of the datasets, indicating that the UV-ozone product should be used with caution here. Below 15 km, the disagreement between datasets is larger, with many sets of comparisons exceeding 50 % relative differences, and similarly above 45 km many sets of comparisons exceed differences of 150 %. Altogether this indicates that the MAESTRO UV-ozone dataset is best used as a stratospheric product. As with the Vis.-ozone comparisons, the absolute and relative differences for the UV-ozone comparisons are summarized in Table 3 for three altitude regimes, corresponding to 15–20 km, 20–45 km, and 45-80 km, chosen to highlight the properties of this product.

The correlation between the coincident measurements is shown in Fig. 8. Across the majority of the comparisons, the largest correlation coefficients are found between approximately 15 and 35 km. Within this range, the best profile-averaged correlation is found with ACE-FTS, with both versions yielding coefficients of 0.88 for sunrise coincident measurements, and above 0.87 for sunset measurements. The lowest average correlation coefficients in this range come from comparisons with SAGE II sunrise measurements, which have an average value of 0.54, with GOMOS sunset measurements, which have an

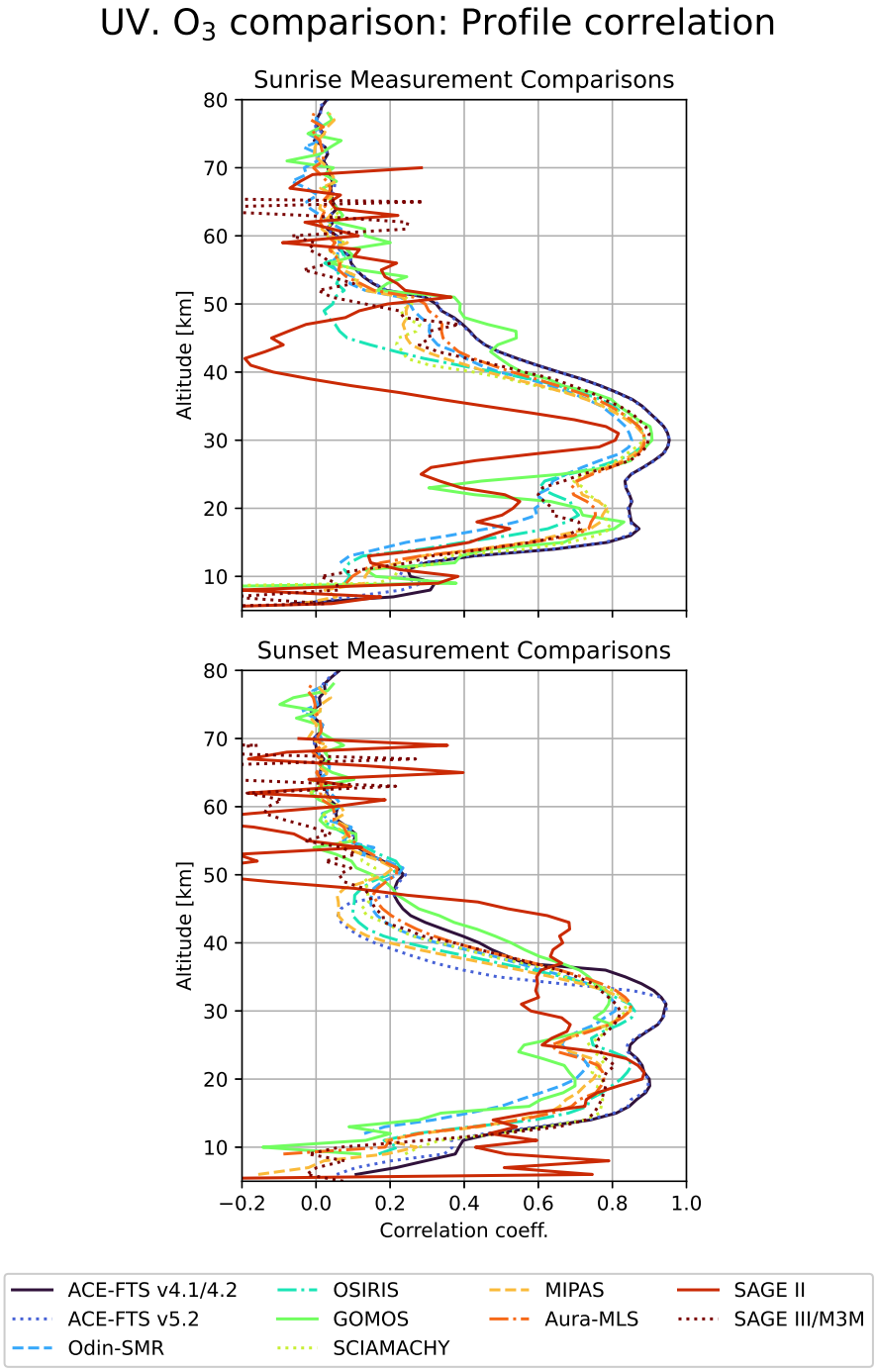

Figure 8. Same as Fig. 4 but for MAESTRO UV-ozone measurements.

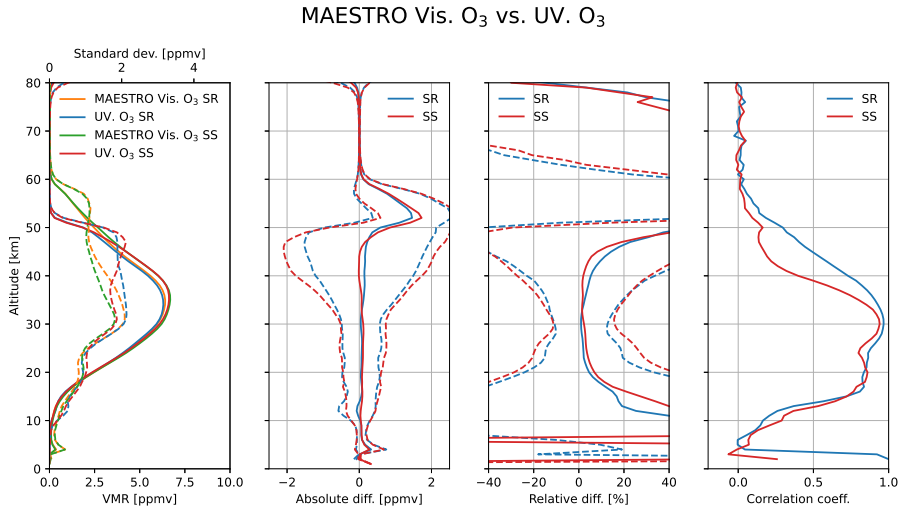

Figure 9. Comparison of the MAESTRO sunrise (SR) and sunset (SS) Vis.-ozone profiles with the MAESTRO UV-ozone profiles. From left to right, the mean sunrise and sunset profiles, the absolute difference, relative difference, and correlation coefficient are shown. The mean profiles are presented using the lower x-axis scale, with the 1σ standard deviations of the profiles shown as dashed lines using the upper x-axis scale.

average value of 0.67, and with Odin-SMR, which has an average coefficient of 0.66 (0.69) during sunrise (sunset). Due to the sparse sampling of the first two datasets, there is a strong likelihood that those comparisons are influenced by sampling bias, contributing to the poor correlation observed. The remaining datasets show average correlation coefficients over this range between 0.72 and 0.79 for sunrise coincident measurements, and between 0.70 and 0.79 for sunset coincident measurements. While the coefficient correlations are somewhat less than for the Vis.-ozone product, the correlation coefficients over this range show that the majority of the datasets are in good agreement with MAESTRO over this range. Outside of the 15 to 35 km range, the correlation coefficients quickly fall to low values, falling to below 0.5 for the majority of the datasets below 13 km and above 42 km. Greater differences are noted with the UV-ozone product between the sunrise and sunset correlation coefficients, with the latter tending toward lower correlation values. Combined with the narrower range of good agreement, the measurement correlation shows that the UV-ozone product should be treated more cautiously than the Vis.-ozone product.

4.2.3 Comparison of MAESTRO Vis.-ozone and UV-ozone

In addition to the comparisons of the two MAESTRO ozone products against other datasets, they can also be compared against each other. As the two products are retrieved independently, this intercomparison allows for an examination of the consistency of the ozone products while removing the influence of geophysical variability. Ahead of this direct product intercomparison, it is also worth noting that a similar minimization of the impact of geophysical variability occurs in the comparisons made between the MAESTRO products and ACE-FTS as the two instruments share a line-of-sight and measure at the same time

using the same observational geometry, allowing direct comparisons to more directly assess the instrumentation and retrieval technique(s). Thus, the excellent agreement observed for both MAESTRO ozone products with ACE-FTS gives confidence in the data treatment and reinforces the viability of these instruments and their ozone data products.

Direct comparisons of the MAESTRO Vis.-ozone and UV-ozone products are shown in Fig. 9. Starting with the mean profiles, the sunrise and sunset profiles are found to be in good agreement from the troposphere up to about 47 km, with the Vis.-ozone product having a slightly larger ozone concentration over this range. Above about 47 km, there is a sharp decrease in the UV-ozone mean concentration, such that the UV product falls to near 0 ppmv by 55 km. In contrast, the Vis.-ozone product more gradually decreases from the stratospheric ozone maximum, only reaching concentrations near 0 ppmv around 60 km. The UV-ozone product is also found to have significantly larger standard deviation profiles between 30 and 53 km, while the standard deviation profiles of the Vis.-ozone product are larger between 53 and 60 km.

Turning to the absolute difference, only small differences are noted below about 47 km and above 60 km, while within this range, the MAESTRO Vis.-ozone is found to be larger than the UV-ozone product due to the differences in behavior observed with altitude for the two products. The relative difference profiles largely reflect these absolute differences, with exception for large differences noted below about 20 km that can be at least partially attributed to the small VMR of ozone at low altitudes that leads small absolute differences to result in large relative differences. Finally, the correlation coefficients are found to be high between about 15 km and either 35 km (sunset) or 40 km (sunrise), which are largely similar to the correlation coefficients shown for the UV-ozone product in Fig. 8.

The loss of signal from the UV channel of MAESTRO likely contributes to the observed differences between the two MAESTRO ozone products. As stated above, the gradual buildup of an unknown contaminant reduced the throughput of the MAESTRO UV channel, such that past 2009 there was insufficient signal for the retrieval of viable products from this channel. However, this was a gradual change over time, rather than a sudden event, and the 2009 end date is empirically determined based on the quality of data retrieved from MAESTRO measurements. As such, there was a gradual decrease in the quality of the products over time, and while the version 4.5 UV products have been thoroughly vetted, this degradation may contribute to the observed differences between the UV-ozone and the Vis.-ozone. The larger standard deviation profiles of the former support a gradual change in the product over time. Between this gradual loss, the sharper decrease in ozone above 50 km and the somewhat more limited range over which good agreement and high correlation is found between the MAESTRO UV-ozone product and that of the other datasets, overall it is found that the Vis.-ozone product is better suited for use in scientific applications.

4.3 UV NO_2

Comparisons between the MAESTRO sunrise and sunset NO_2 data against the diurnally-scaled (where required) coincident measurements from the other datasets are shown in Figs. 10 through 13. As with the UV-ozone data, the MAESTRO NO_2 measurements are only viable for a portion of the MAESTRO operational period; in this case from the start of the mission through to June 2009. As a result of this, as well as not all of the datasets employed in this study having a NO_2 product, only eight sets of comparisons can be made, with none being made with Odin-SMR, Aura-MLS, OMPS-LP or SAGE III/ISS.

4.3.1 Profile overview

The mean sunrise and sunset MAESTRO and coincident comparison profiles, and their standard deviations, are shown in Fig. 10. Across the eight sets of profiles, the shape of the mean NO_2 profile is generally consistent below approximately 45 km, with the mean profiles showing an increasing concentration with altitude from the troposphere up to a maximum near 35 km. Above this maximum, the NO_2 concentration begins to decrease with altitude; however around 45 km the datasets begin to differ from each other, with two datasets (OSIRIS and SCIAMACHY) truncating at this altitude, two sunset profiles (SAGE II and SAGE III/M3M) showing fairly fixed NO_2 concentrations with altitude, and with the remaining profiles continuing to decrease with altitude. As with ozone, the MAESTRO NO_2 mean profiles show a sharper decrease in concentration with altitude than the comparison datasets, with this deviation occurring around 45 km. Here, MAESTRO NO_2 quickly decreases to near 0 ppbv, as does its standard deviation. Above 70 km the MAESTRO profiles increase with altitude; however, only MIPAS has NO_2 measurements past 50 km and this mesospheric feature is not observed in the MIPAS data.

Around the stratospheric NO_2 peak, large differences are found in the mean profile trace gas concentrations, with peak values ranging from just over 2 ppbv up to about 7.5 ppbv around 35 km. Along with the large spread in mean profile concentrations between the datasets, the sunrise and sunset profiles are found to consistently differ from each other for each of the datasets, with the latter yielding larger NO_2 VMR values throughout the majority of the stratosphere. Unlike with the ozone profiles, a more pronounced difference in the sunrise and sunset profiles due to the diurnal cycle of NO_2 is expected; however, the scale of these differences between the different sets of comparisons show the potential for sampling biases to impact these comparisons in the less densely sampled, non-ACE-FTS datasets. Despite the variability in the mean profiles, all but one of the comparisons (SAGE II sunrise) indicate that MAESTRO NO_2 is low biased in the stratosphere compared to the other datasets. This low bias is most clearly illustrated in comparisons made with OSIRIS, GOMOS, and SCIAMACHY. The differing behavior observed with the SAGE II sunrise NO_2 dataset can be at least partially attributed to the thermal shock the instrument experiences during measurement events, which can be readily accounted for in sunset measurements but requires a correction to be applied for the sunrise measurements (Damadeo et al., 2013). Around the stratospheric NO_2 maximum, most of the datasets also display their largest standard deviations; however there is some variation as to the exact altitude where the largest values occur. Both of the SAGE II profiles, as well as the SAGE III/M3M sunset profile, show their largest standard deviation values between 40 and 50 km; however, this is likely associated with retrieval-boundary uncertainty effects and the aforementioned thermal shock for the former.

Despite the low bias of the mean MAESTRO profiles, the standard deviation profiles for the MAESTRO NO_2 product show general agreement in the stratosphere with those from the comparison instruments. Above 70 km, the MAESTRO dataset displays extremely large standard deviation values in association with the aforementioned mesospheric NO_2 feature, with standard deviation values in excess of 10 ppbv. This large upper atmospheric variability, coupled to the large NO_2 concentrations not observed elsewhere, indicates that this secondary NO_2 feature in the MAESTRO dataset might be an artifact caused by the retrieval. The exact cause of this is likely due to the over-constraining of the retrieval in the lower mesosphere, as observed

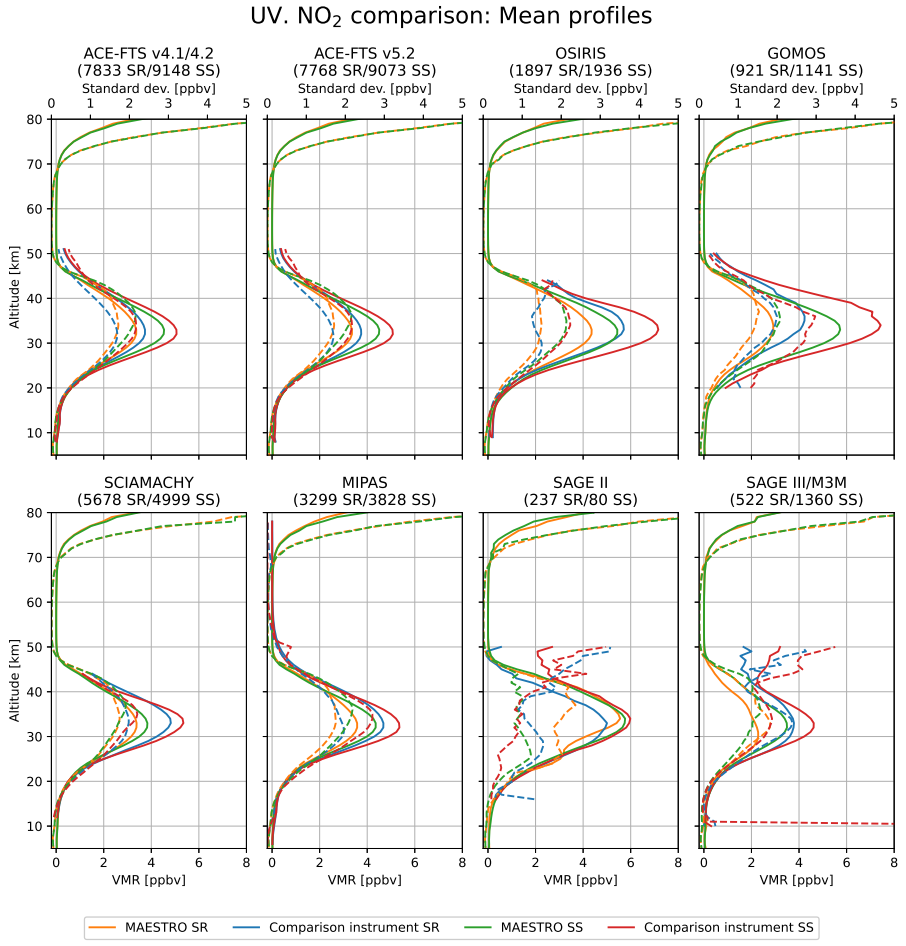

Figure 10. Same as Fig. 1 but for MAESTRO UV NO_2 measurements.

with the ozone products from MAESTRO, coupled to an under-constrained region, namely the span from 70 km upward, into which the NO_2 is partitioned.

Focusing on the individual sets of comparisons, the best agreement is found between MAESTRO and the ACE-FTS version 4.1/4.2 and version 5.2 datasets. The NO_2 from all three datasets is found to peak at the same altitude in the stratosphere, and for both sets of comparisons the sunset measurements are found to be about 1 ppbv larger than the sunrise measurements at this point, which is expected given the diurnal cycle in NO_2. The standard deviation profiles from ACE-FTS and MAESTRO are also found to follow a similar shape, with the sunrise profiles peaking near the VMR maximum, while the sunset profiles peak closer to 37 km, showing a consistency in the representation of NO_2 between the datasets. However, despite these shared properties, there is a difference of about 0.3 ppbv between the mean MAESTRO and ACE-FTS profiles, which persists from about 28 km up to 40 km. The magnitude of this difference is unexpected given the shared line-of-sight of ACE-FTS and MAESTRO, as well as results from pre-flight tests of the two instruments that showed agreement to within 0.5 % for mea-

surements of NO_2 (Dufour et al., 2006). A contributing factor for this difference is likely the lack of temperature corrections for the MAESTRO data in the NO_2 retrieval. Additionally, while the MAESTRO mean NO_2 is found to be smaller than that of ACE-FTS, the standard deviation of the MAESTRO dataset is slightly larger than that of ACE-FTS indicating it is a more variable product.

The GOMOS comparisons are generally similar to those with ACE-FTS, albeit with three main differences. The first difference is in the magnitude of the mean sunset NO_2 profile; both the GOMOS sunset profile and the MAESTRO sunset profile show higher NO_2 concentrations around the stratospheric NO_2 maximum, by about 2 ppbv and 1.5 ppbv respectively, as compared to the same type of profile from the ACE-FTS datasets. The second difference is in the location of the stratospheric NO_2 peak, with the two GOMOS profiles peaking approximately 2 km higher than those seen in the ACE-FTS comparisons. Despite this, the standard deviation profiles reach their maximum value at a higher altitude for the sunset profiles, as observed with ACE-FTS. The final difference is in the general agreement between the MAESTRO and GOMOS profiles, which shows a larger absolute difference over the stratosphere than what was observed for ACE-FTS, with differences near the stratospheric peak of 1.5–2 ppbv.

Broadly the OSIRIS, SCIAMACHY, and MIPAS comparisons share similar properties with each other, which differentiate these comparisons from those above. Most notably, for each of the comparison datasets both the mean sunset and sunrise NO_2 profiles are found to be larger than both of the coincident profiles from MAESTRO, with an approximately 1–2 ppbv difference between the comparison and MAESTRO profiles around the stratospheric maximum. Despite this, the general relationship between the sunrise and sunset profiles, wherein the latter is larger than the former, is maintained in these comparisons. The three sets of comparisons also show some significant points of difference from each other. This includes the sunset profiles from the OSIRIS comparisons having larger mean VMR values than the MIPAS or SCIAMACHY comparisons by 1–2 ppbv, and the sunrise standard deviation profiles from the OSIRIS comparisons having the smallest standard deviation profiles of the three. Additionally, the MIPAS dataset has NO_2 information up to 79 km, unlike the other comparison datasets; however, above 50 km these retrieved values are consistently very small, unlike those of MAESTRO, showing no agreement with the MAESTRO high-altitude NO_2 feature.

Finally, the SAGE II and SAGE III/M3M comparisons are shown to differ significantly from what is seen with the other comparisons. Starting with the similarities with the other comparisons, the SAGE II and SAGE III/M3M mean profiles have larger NO_2 concentrations for the sunset measurements than for the sunrise, and the mean profiles show a peak in NO_2 around 35 km. SAGE III/M3M shows larger NO_2 concentrations than MAESTRO throughout the majority of the stratosphere, in line with the other comparisons, but the SAGE II sunrise comparison shows that MAESTRO has higher NO_2 concentrations above about 30 km. Additionally, the sunset comparisons show little difference between the MAESTRO and SAGE II mean profiles, resulting in the best agreement of any dataset. Further differences from the other datasets include the mean SAGE II and SAGE III/M3M profiles increasing above 45 km, the standard deviation profiles for SAGE II and the coincident MAESTRO profiles not following the general shape of the other datasets, and the two SAGE datasets showing an increase in their standard deviation above about 40 km. Despite these differences, SAGE III/M3M shows a 1–1.5 ppbv difference throughout much of the stratosphere from MAESTRO NO_2, similar to what is observed with the other comparisons, and it is only the SAGE II

comparisons that show strong disagreement with the other datasets as to the bias of MAESTRO NO_2. As with the comparisons made for the MAESTRO ozone products, the comparisons made with SAGE II are likely influenced by the low number of coincident profiles found between the two datasets, with only 317 set of profiles compared. This, in addition to the thermal shock effect discussed above, indicates that the comparisons with SAGE II should still be treated cautiously due to the potential impact of sampling biases (Damadeo et al., 2013).

4.3.2 Comparison metrics

The absolute and relative difference between the datasets are shown in Figs. 11 and 12 respectively. From these comparisons, particularly from the relative difference plots, the best agreement between MAESTRO and the comparison instruments is found to be between approximately 20 and 40 km. Below 20 km, the comparisons tend to show oscillating differences, with many of the comparisons indicating a low bias for the MAESTRO NO_2 dataset while a few indicate a high bias for at least part of the profile. The oscillations in these differences are not solely due to limited numbers of comparison profiles as they are observed for comparisons with both many (e.g., ACE-FTS) and few (e.g., SAGE III/M3M) coincident measurements. Neglected diurnal variations along the line-of-sight in the retrievals of the instruments examined may contribute to these low altitude differences (e.g., Dubé et al., 2021). Between 20 km and 40 km, a more distinct low bias is noted for MAESTRO as compared to most of the comparison datasets. Above 40 km, most of the datasets yield average relative differences in excess of 60 %, showing poor agreement with the MAESTRO retrievals above the middle stratosphere.

Focusing between 20 and 40 km, where the comparison datasets show the best agreement, the overall closest agreement is found with the SAGE II measurements coincident with the sunset MAESTRO measurements, which have an average absolute difference of 0.20 ppbv and a relative difference of 8.5 %. However, the robustness of this finding is brought into question are there are only 80 sunset coincident profiles between the two datasets. The next closest agreement is found with ACE-FTS version 4.1/4.2 and version 5.2, which have sunrise (sunset) absolute differences of 0.25 (0.35) and 0.28 (0.37) ppbv respectively. These translates into mean relative differences from the MAESTRO sunrise (sunset) measurements of 15.7 (14.3) % for ACE-FTS version 4.1/4.2 and 15.9 (14.4) % for ACE-FTS version 5.2. This difference is larger than what is expected from pre-flight tests of the instruments (Dufour et al., 2006), but the high degree of agreement observed, as compared to other datasets, follows from the minimization of the effects of geophysical variability as the two instrument share the same line-of-sight and measurement times.

Despite larger average absolute differences, ranging from 0.50 to 0.76 ppbv, the MIPAS sunset, OSIRIS sunrise, and SAGE II sunrise comparisons all show decent agreement, to within 19.2 %, with MAESTRO as well. For sunset-coincident MIPAS measurements, the average relative difference is 16.2 %, while for OSIRIS sunrise coincident measurements the average relative difference is 19.2 %, and for SAGE II sunrise coincident measurements it is 12.0 %. The OSIRIS sunset coincident measurements show the second largest absolute difference, of 1.02 ppbv,, but due to this set of comparisons possessing the highest average VMRs, this is only a 23.6 % difference from what is observed with the coincident MAESTRO sunset measurements. The remaining coincident comparisons all have larger absolute and relative differences, with mean relative differences in excess of 20.9 % over this 20 km span.

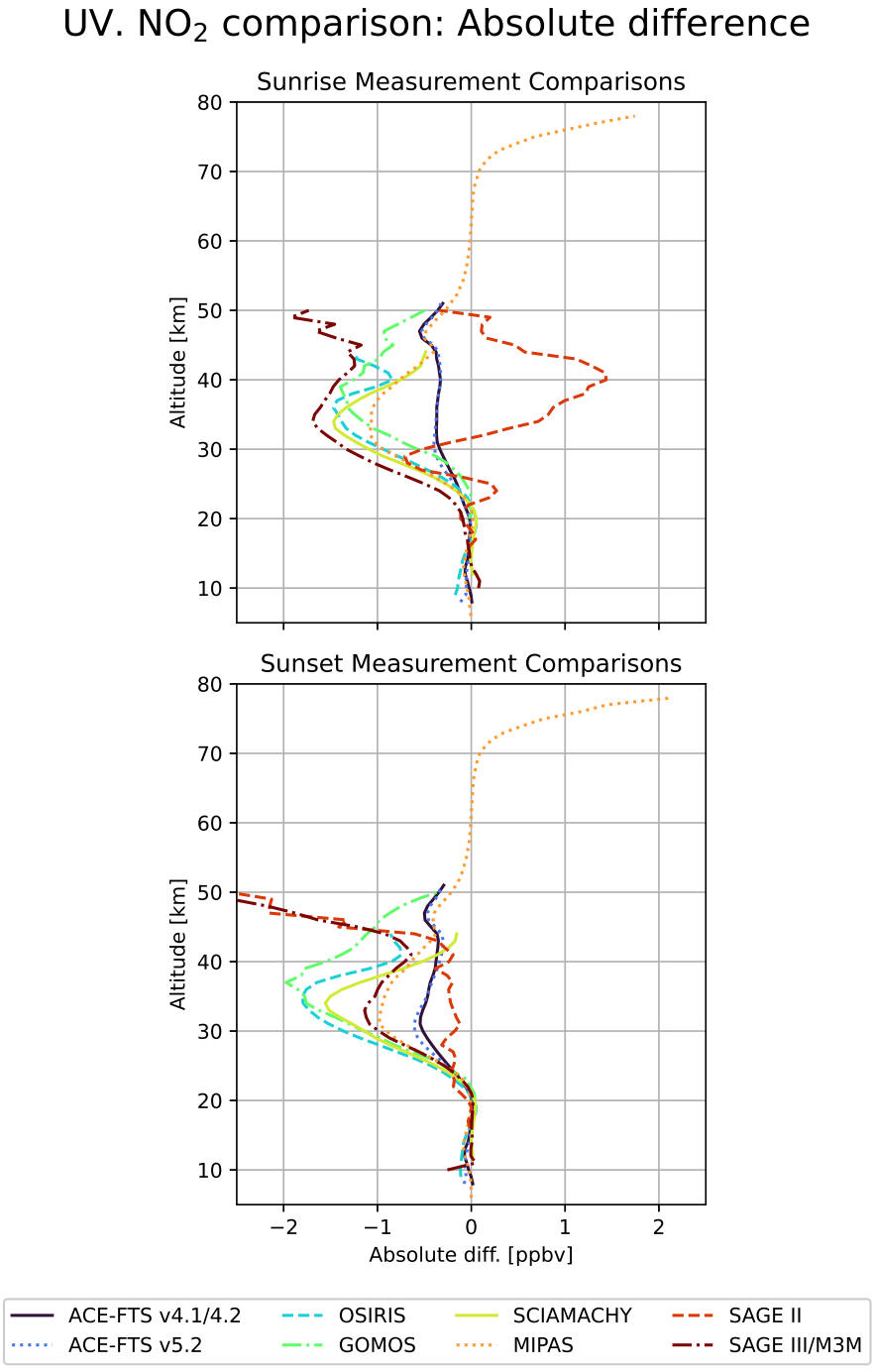

Figure 11. Same as Fig. 2 but for MAESTRO UV NO_2 measurements.

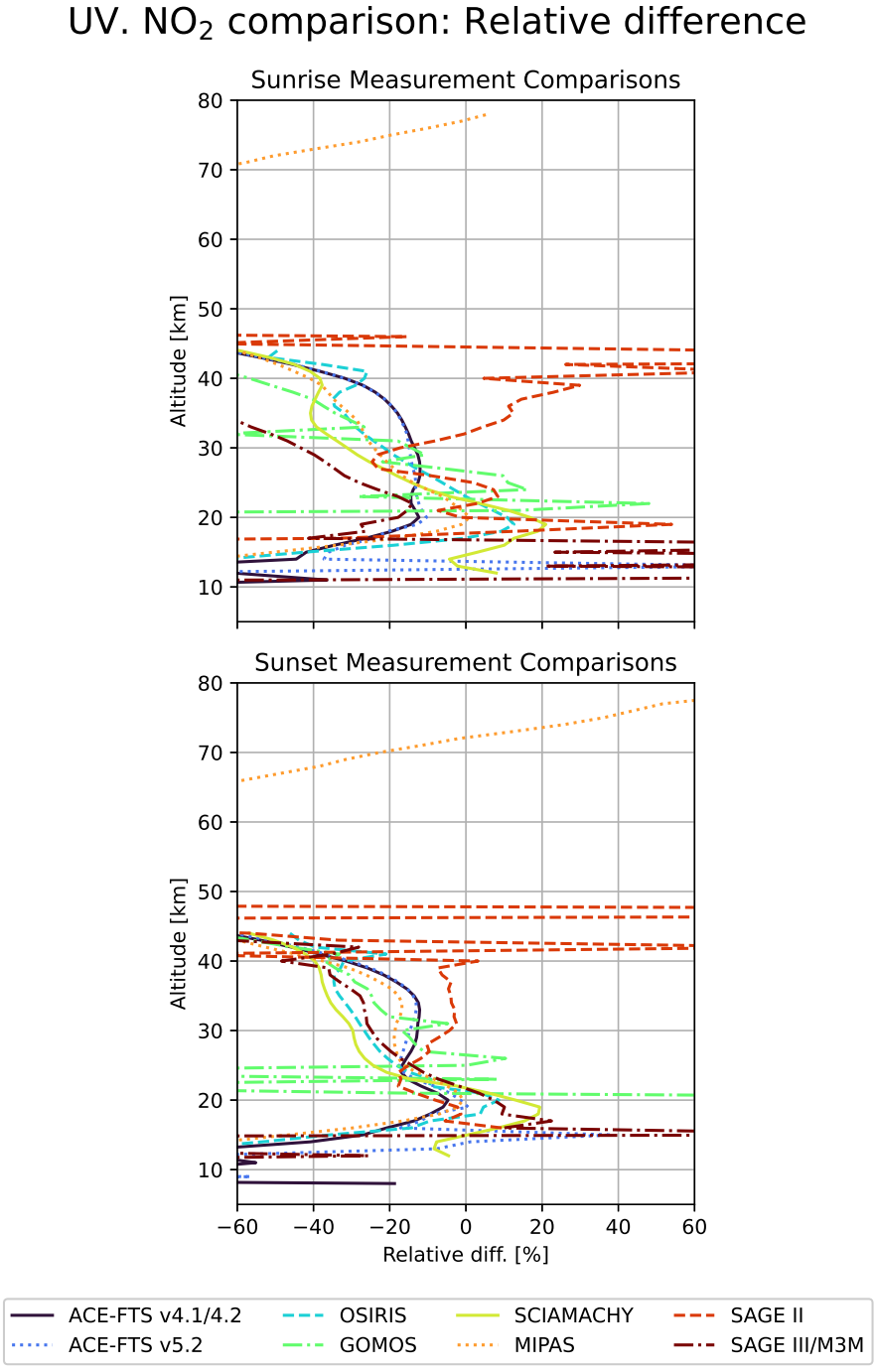

Figure 12. Same as Fig. 3 but for MAESTRO UV NO_2 measurements.

Table 4. Same as Table 2 but for MAESTRO NO_2. Note that for GOMOS, there is no data below 20 km, resulting in the empty entries in the table. Additionally, not all datasets reach up to 60 km, and so where this is the case, the average is presented up to the maximum available altitude.

Alt. range	15–20 km		20–40 km		40–60 km	
Metric	Mean Δ_{abs} (ppbv)	Mean Δ_{rel} (%)	Mean Δ_{abs} (ppbv)	Mean Δ_{rel} (%)	Mean Δ_{abs} (ppbv)	Mean Δ_{rel} (%)
ACE-FTS v4.1/4.2	0.02 (0.01)	27.3 (15.4)	0.25 (0.35)	15.7 (14.3)	0.40 (0.40)	102.3 (101.4)
ACE-FTS v5.2	0.02 (0.01)	25.0 (15.4)	0.28 (0.37)	15.9 (14.4)	0.39 (0.36)	102.1 (100.9)
OSIRIS	0.04 (0.04)	16.7 (13.6)	0.76 (1.02)	19.2 (23.6)	1.04 (0.81)	38.3 (36.5)
GOMOS	-	-	0.60 (1.00)	42.3 (42.9)	0.92 (1.00)	120.0 (99.0)
MIPAS	0.03 (0.03)	22.3 (20.4)	0.65 (0.60)	20.9 (16.2)	0.31 (0.26)	128.0 (127.8)
SCIAMACHY	0.02 (0.03)	13.1 (12.6)	0.79 (0.83)	26.6 (27.2)	0.59 (0.29)	47.1 (46.9)
SAGE II	0.03 (0.02)	90.8 (4.6)	0.50 (0.20)	12.0 (8.5)	0.66 (1.22)	137.4 (151.3)
SAGE III/M3M	0.05 (0.01)	52.5 (34.7)	1.03 (0.66)	43.4 (21.0)	1.45 (1.44)	143.9 (113.0)

Between 15 and 20 km, where the relative difference profiles begin to show oscillating comparison values, somewhat decent agreement is observed with some of the datasets, particularly for the sunset comparisons. In this range, the ACE-FTS sunset, OSIRIS, MIPAS sunset, SCIAMACHY, and SAGE II sunset comparisons are all found to yield agreement with MAESTRO to within 20.4 %; with the SAGE II sunset comparisons showing the best overall average agreement to within 4.6 %. However, many of the comparisons fare more poorly, with relative differences ranging from 22.3 % to 90.8 %. These large relative differences are largely impacted by the low NO_2 concentrations in this region, which causes small absolute differences to lead to large relative differences between the datasets. The average absolute differences with all comparison datasets within this region span from 0.01 to 0.05 ppbv. These results indicate that there remains a degree of agreement between 15 and 20 km, but caution is required in using the MAESTRO dataset within this range. The absolute and relative differences for the NO_2 comparisons are summarized in Table 4 for three altitude regimes chosen to highlight the properties of this product.

Figure 13 shows the correlation between MAESTRO and the comparison datasets. The vertical range with the best correlation for most datasets is approximately 15 to 40 km. Within this span, the highest correlation is found with the two versions of ACE-FTS, which have a sunrise (sunset) measurement correlation of at least 0.87 (0.89). Over this range, the OSIRIS sunset, SCIAMACHY, MIPAS, and SAGE III/M3M comparisons all have an average correlation above 0.75. The OSIRIS sunrise comparison is somewhat worse overall, with an average correlation of 0.65, and GOMOS also has lower correlation, at 0.60 (0.59) for the sunrise (sunset) comparison, due to the poor correlation found between it and MAESTRO between 20 and 25 km. Likely influenced by the few coincident profiles, as well as a systematic difference in sampling location, the SAGE II average sunrise correlation is only 0.49 for this range, and the sunset comparisons are found to be uncorrelated, with an average correlation coefficient of -0.03. However, despite this variable level of agreement, most datasets show generally moderate or good correlation over this range. Outside of this range, the correlation of most of the datasets quickly falls to below 0.50, with the

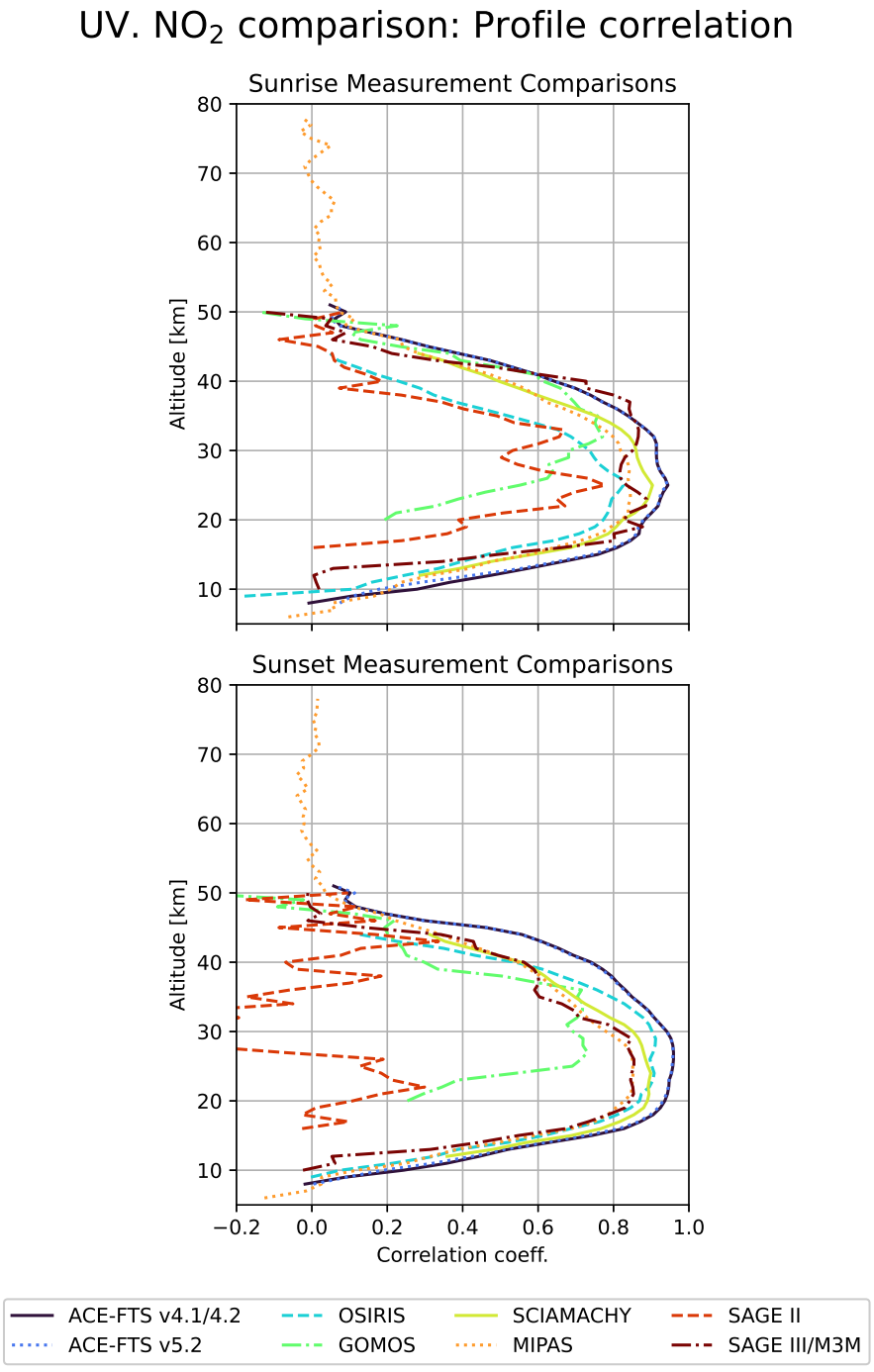

Figure 13. Same as Fig. 4 but for MAESTRO UV NO_2 measurements.

majority of the datasets reaching this threshold between 11 and 13 km, and between 41 and 43 km. The drop in correlation coefficients outside of the 15–40 km range, along with the calculated relative and absolute differences, indicates that the NO_2 product should primarily be used in the lower and middle stratosphere.

5 Conclusions

In this study, the recently released version 4.5 ozone and NO_2 retrieval products from MAESTRO have been compared against coincident measurements for validation purposes. Twelve datasets were used for these comparisons; however only the Vis.-ozone product from MAESTRO was assessed using all 12 datasets due to the limited viability of MAESTRO UV products, which span only from the start of the ACE mission until 2009, and the lack of a NO_2 product from two of the instruments employed.

Before addressing the individual products, it is crucial to note that for all three MAESTRO products, the best agreement is generally found with ACE-FTS. This agreement is important due to the two instruments sharing a line-of-sight while employing different measurement techniques and retrieval schemes. As the shared line-of-sight eliminates the majority of the influence of geophysical variability on the measurements compared, the differences between the two sets of products arises almost entirely from instrumental and retrieval technique differences. Thus, we can conclude that the two instruments are largely consistent and both instruments likely have good retrieval techniques.

The Vis.-ozone product was found to have excellent agreement with the coincident datasets, with average relative differences between 2.3 and 8.2 % from 20 to 50 km, and high correlation coefficients, generally in excess of 0.71, between 15 and 40 km. The UV-ozone product from MAESTRO was found to agree slightly less well with the coincident datasets, with average relative differences between 20 and 45 km of 2.8 to 11.9 %. From 15 to 35 km, good correlation was found between the UV-ozone product and the coincident datasets, with correlation coefficients typically in excess of 0.70 on average. Both datasets show a small high bias in the stratosphere, as compared to the comparison instruments. Despite the good agreement found over the stratosphere, both MAESTRO ozone products have been found to show significant differences from the other datasets in the mesosphere. Analysis of the mean ozone profiles constructed from the MAESTRO ozone profiles, and the standard deviation thereof, indicated that the MAESTRO version 4.5 retrieval appears to over-constrain the ozone concentration in the mesosphere, resulting in the near 0 ppmv concentrations observed over this region which show considerable disagreement with those from the other datasets. Thus scientific application of the MAESTRO ozone products should limit their use outside of the stratosphere.

Finally, UV NO_2 from MAESTRO was found to agree with the majority of the comparison datasets to within 27.2 % between 20 and 40 km, with the relative differences ranging from 8.5 to 43.4 % on average over this span. A distinct low bias was identified for this product over the stratosphere. From 15 to 40 km, good correlation was found with most of the comparison datasets, with almost all of the comparison sets having average correlation coefficients over 0.70. The low bias observed over the stratosphere, coupled to a large concentration of NO_2 in the mesosphere, appears to be influenced by inaccurate partitioning of NO_2 in the MAESTRO version 4.5 retrieval, which seemingly results in the accumulation of NO_2

above 70 km in the profiles. When coupled to the limited range over which decent agreement is found with the comparison datasets, this indicates that the MAESTRO NO_2 product should be only be used in the lower and middle stratosphere.

Overall, the findings presented in this work support the use of the MAESTRO version 4.5 dataset for stratospheric studies. The Vis.-ozone product is viable from the start of the ACE mission (February 2004) through to the present and their usage should principally be confined to between 20 and 50 km. This Vis.-ozone product is the preferred MAESTRO ozone product for general applications, due to the UV-ozone products only being viable until December 2009 and over a slightly narrower stratospheric range from 20 to 45 km; however, for studies focusing on UV-derived measurements of ozone, it is a valid dataset for consideration. Finally, the MAESTRO NO_2 product is found to be only viable from the start of the mission until June 2009 and general agreement with other datasets is only achieved between 20 and 40 km. So long as applications for this product are able to work within this limited range of viability, then the MAESTRO NO_2 product should be suitable for scientific applications.

Data availability. MAESTRO version 4.5, as well as ACE-FTS version 4.1/4.2 and version 5.2 data, are available from https://databace.scisat.ca/level2/ (last access: 10 June 2024; MAESTRO; ACE-FTS, a, b). Access to these products requires registration. Data quality flags for ACE-FTS version 4.1/4.2 and version 5.2 are available from https://doi.org/10.5683/SP2/BC4ATC (Sheese and Walker, 2023a) and https://doi.org/10.5683/SP3/NAYNFE (Sheese and Walker, 2023b). OSIRIS version 7.2 ozone data are available at ftp://odin-osiris.usask.ca/ (last access: 10 June 2024; OSIRIS). Odin-SMR version 3.0 data are available from https://odin.rss.chalmers.se/level2 (last access: 10 June 2024; European Space Agency). GOMOS IPF version 6.01 data are available from ftp://gomo-ftp-ds.eo.esa.int/ (last access: 11 June 2024; European Space Agency, 2017). Access requires registration. SCIAMACHY IUP version 3.5 data are available from ftp://scia-ftp-ds.eo.esa.int (last access: 11 June 2024; European Space Agency, 2016). Access requires registration. MIPAS IMK-IAA version 8 data are available from https://imk-asf-mipas.imk.kit.edu/ (last access: 11 June 2024; MIPAS IMK-IAA). Access requires registration. OMPS-LP version 2.6 ozone data are available from https://doi.org/10.5067/8MO7DEDYTBH7 (last access: 11 June 2024; Kramarova, 2023). Access requires registration. Aura-MLS version 5.3 ozone data are available from https://disc.gsfc.nasa.gov/datacollection/ML2O3_NRT_005.html (last access: 11 June 2024; EOS MLS Science Team, 2022). Access requires registration. SAGE II version 7.0 data are available from https://asdc.larc.nasa.gov/project/SAGE%20II (last access: 11 June 2024; NASA/LARC/SD/ASDC, 2012), SAGE III/M3M version 4 data are available from https://asdc.larc.nasa.gov/project/SAGE%20III-M3M (last access: 11 June 2024; NASA/LARC/SD/ASDC, 2009), and SAGE III/ISS version 5.3 data are available from https://asdc.larc.nasa.gov/project/SAGE%20III-ISS (last access: 11 June 2024; NASA/LARC/SD/ASDC). Access requires registration. The diurnal scaling factors used in this study are available from https://avdc.gsfc.nasa.gov/pub/data/project/GMI_SF/ (last access: 3 August 2023; Strode, 2021)

Author contributions. This study was designed by PSJ with input from JRD, CTM, KAW, and JZ. PSJ wrote the manuscript and performed the analyses. CTM and JZ provided their expertise on MAESTRO. Valuable comments on the manuscript were provided by all authors.

Competing interests. The authors declare that they have no conflict of interest.

Acknowledgements. This project is supported by a grant from the Canadian Space Agency (CSA). The Atmospheric Chemistry Experiment (ACE), also known as SCISAT, is a Canadian-led mission mainly supported by CSA. We thank Peter Bernath for his leadership of the ACE mission. Odin is a Swedish-led satellite project funded jointly by Sweden (Swedish National Space Board), Canada (CSA), France (Centre National d'Études Spatiales), and Finland (Tekes), with support by the Third Party Missions program of the European Space Agency (ESA). The SAGE II, SAGE III/M3M, and SAGE III/ISS data were obtained from the NASA Langley Research Center Atmospheric Science Data Center. We would like to thank Patrick Sheese for aiding with the SCIAMACHY data co-located with MAESTRO/ACE-FTS measurements.

References

ACE-FTS: ACE-FTS Version 4.1/4.2 Level 2 Data [data set], available at: https://databace.scisat.ca/level2/, last access: 10 June 2024, a.

ACE-FTS: ACE-FTS Version 5.2 Level 2 Data [data set], available at: https://databace.scisat.ca/level2/, last access: 10 June 2024, b.

Adams, C., Strong, K., Batchelor, R. L., Bernath, P. F., Brohede, S., Boone, C., Degenstein, D., Daffer, W. H., Drummond, J. R., Fogal, P. F., Farahani, E., Fayt, C., Fraser, A., Goutail, F., Hendrick, F., Kolonjari, F., Lindenmaier, R., Manney, G., McElroy, C. T., McLinden, C. A., Mendonca, J., Park, J.-H., Pavlovic, B., Pazmino, A., Roth, C., Savastiouk, V., Walker, K. A., Weaver, D., and Zhao, X.: Validation of ACE and OSIRIS ozone and NO_2 measurements using ground-based instruments at 80° N, Atmos. Meas. Tech., 5, 927–953, https://doi.org/10.5194/amt-5-927-2012, 2012.

Adams, C., Bourassa, A. E., Bathgate, A. F., McLinden, C. A., Lloyd, N. D., Roth, C. Z., Llewellyn, E. J., Zawodny, J. M., Flittner, D. E., Manney, G. L., Daffer, W. H., and Degenstein, D. A.: Characterization of Odin-OSIRIS ozone profiles with the SAGE II dataset, Atmos. Meas. Tech., 6, 1447–1459, https://doi.org/10.5194/amtd-6-1033-2013, 2013.

Adams, C., Bourassa, A. E., Sofieva, V., Froidevaux, L., McLinden, C. A., Hubert, D., Lambert, J.-C., Sioris, C. E., and Degenstein, D. A.: Assessment of Odin-OSIRIS ozone measurements from 2001 to the present using MLS, GOMOS, and ozonesondes, Atmos. Meas. Tech., 7, 49–64, https://doi.org/10.5194/amt-7-49-2014, 2014.

Bauer, R., Rozanov, A., McLinden, C. A., Gordley, L. L., Lotz, W., Russell III, J. M., Walker, K. A., Zawodny, J. M., Ladstätter-Weißenmayer, A., Bovensmann, H., and Burrows, J. P.: Validation of SCIAMACHY limb NO_2 profiles using solar occultation measurements, Atmos. Meas. Tech., 5, 1059–1084, https://doi.org/10.5194/amt-5-1059-2012, 2012.

Bernath, P. F.: The Atmospheric Chemistry Experiment (ACE), J. Quant. Spectrosc. Ra., 186, 3–16, https://doi.org/10.1016/j.jqsrt.2016.04.006, 2017.

Bernath, P. F., McElroy, C. T., Abrams, M. C., Boone, C. D., Butler, M., Camy-Peyret, C., Carleer, M., Clerbaux, C., Coheur, P.-F., Colin, R., DeCola, P., DeMazière, M., Drummond, J. R., Dufour, D., Evans, W. F. J., Fast, H., Fussen, D., Gilbert, K., Jennings, D. E., Llewellyn, E. J., Lowe, R. P., Mahieu, E., McConnell, J. C., McHugh, M., McLeod, S. D., Michaud, R., Midwinter, C., Nassar, R., Nichitiu, F., Nowlan, C., Rinsland, C. P., Rochon, Y. J., Rowlands, N., Semeniuk, K., Simon, P., Skelton, R., Sloan, J. J., Soucy, M.-A., Strong, K., Tremblay, P., Turnbull, D., Walker, K. A., Walkty, I., Wardle, D. A., Wehrle, V., Zander, R., and Zou, J.: Atmospheric Chemistry Experiment (ACE): Mission overview, Geophys. Res. Lett., 32, L15S01, https://doi.org/10.1029/2005GL022386, 2005.

Bertaux, J. L., Kyrölä, E., Fussen, D., Hauchecorne, A., Dalaudier, F., Sofieva, V., Tamminen, J., Vanhellemont, F., Fanton d'Andon, O., Barrot, G., Mangin, A., Blanot, L., Lebrun, J. C., Pérot, K., Fehr, T., Saavedra, L., Leppelmeier, G. W., and Fraisse, R.: Global ozone monitoring by occultation of stars: an overview of GOMOS measurements on ENVISAT, Atmos. Chem. Phys., 10, 12 091–12 148, https://doi.org/10.5194/acp-10-12091-2010, 2010.

Bognar, K., Zhao, X., Strong, K., Boone, C. D., Bourassa, A. E., Degenstein, D. A., Drummond, J. R., Duff, A., Goutail, F., Griffin, D., Jeffery, P. S., Lutsch, E., Manney, G. L., McElroy, C. T., McLinden, C. A., Millán, L. F., Pazmino, A., Sioris, C. E., Walker, K. A., and Zou, J.: Updated validation of ACE and OSIRIS ozone and NO2 measurements in the Arctic using ground-based instruments at Eureka, Canada, J. Quant. Spectrosc. Ra., 238, 106 571, https://doi.org/10.1016/j.jqsrt.2019.07.014, 2019.

Bognar, K., Tegtmeier, S., Bourassa, A., Roth, C., Warnock, T., Zawada, D., and Degenstein, D.: Stratospheric ozone trends for 1984–2021 in the SAGE II–OSIRIS–SAGE III/ISS composite dataset, Atmos. Chem. Phys., 22, 9553–9569, https://doi.org/10.5194/acp-22-9553-2022, 2022.

Boone, C. D., Nassar, R., Walker, K. A., Rochon, Y., McLeod, S. D., Rinsland, C. P., and Bernath, P. F.: Retrievals for the atmospheric chemistry experiment Fourier-transform spectrometer, Appl. Optics., 44, 7218–7231, https://doi.org/10.1364/AO.44.007218, 2005.

Boone, C. D., Walker, K. A., and Bernath, P. F.: Version 3 retrievals for the Atmospheric Chemistry Experiment Fourier Transform Spectrometer (ACE-FTS), in: The Atmospheric Chemistry Experiment ACE at 10: A Solar Occultation Anthology, pp. 103–127, A. Deepak Publishing, Hampton, Virginia, U.S.A., 2013.

Boone, C. D., Bernath, P. F., Cok, D., Jones, S. C., and Steffen, J.: Version 4 retrievals for the atmospheric chemistry experiment Fourier transform spectrometer (ACE-FTS) and imagers, J. Quant. Spectrosc. Ra., 247, 106 939, https://doi.org/10.1016/j.jqsrt.2020.106939, 2020.

Boone, C. D., Bernath, P. F., and Lecours, M.: Version 5 retrievals for ACE-FTS and ACE-imagers, J. Quant. Spectrosc. Ra., 310, 108 749, https://doi.org/10.1016/j.jqsrt.2023.108749, 2023.

Bourassa, A. E., Degenstein, D. A., Randel, W. J., Zawodny, J. M., Kyrölä, E., McLinden, C. A., Sioris, C. E., and Roth, C. Z.: Trends in stratospheric ozone derived from merged SAGE II and Odin-OSIRIS satellite observations, Atmos. Chem. Phys., 14, 6983–6994, https://doi.org/10.5194/acp-14-6983-2014, 2014.

Bovensmann, H., Burrows, J. P., Buchwitz, M., Frerick, J., Noël, S., Rozanov, V. V., Chance, K. V., and Goede, A. P. H.: SCIAMACHY: Mission Objectives and Measurement Modes, J. Atmos. Sci., 56, 127–150, https://doi.org/10.1175/1520-0469(1999)056<0127:SMOAMM>2.0.CO;2, 1999.

Brasseur, G. P. and Solomon, S.: Aeronomy of the middle atmosphere: Chemistry and physics of the stratosphere and mesosphere, Springer Netherlands, Dordrecht, Great Britain, 3rd edn., 2005.

Buehner, M., McTaggart-Cowan, R., Beaulne, A., Charette, C., Garand, L., Heilliette, S., Lapalme, E., Laroche, S., Macpherson, S. R., Morneau, J., and Zadra, A.: Implementation of deterministic weather forecasting systems based on ensemble–variational data assimilation at Environment Canada. Part I: The global system, Mon. Weather Rev., 143, 2532–2559, https://doi.org/10.1175/MWR-D-14-00354.1, 2015.

Burrows, J. P., Hölzle, E., Goede, A. P. H., Visser, H., and Fricke, W.: SCIAMACHY—scanning imaging absorption spectrometer for atmospheric chartography, Acta Astronaut., 35, 445–451, https://doi.org/10.1016/0094-5765(94)00278-T, 1995.

Chin, M., Ginoux, P., Kinne, S., Torres, O., Holben, B. N., Duncan, B. N., Martin, R. V., Logan, J. A., Higurashi, A., and Nakajima, T.: Tropospheric Aerosol Optical Thickness from the GOCART Model and Comparisons with Satellite and Sun Photometer Measurements, J. Atmos. Sci., 59, 461–483, https://doi.org/10.1175/1520-0469(2002)059<0461:TAOTFT>2.0.CO;2, 2002.

Chu, W. P., McCormick, M. P., Lenoble, J., Brogniez, C., and Pruvost, P.: SAGE II inversion algorithm, J. Geophys. Res.: Atmos., 94, 8339–8351, https://doi.org/10.1029/JD094iD06p08339, 1989.

Colarco, P., da Silva, A., Chin, M., and Diehl, T.: Online simulations of global aerosol distributions in the NASA GEOS-4 model and comparisons to satellite and ground-based aerosol optical depth, J. Geophys. Res.: Atmos., 115, https://doi.org/10.1029/2009JD012820, 2010.

Damadeo, R. P., Zawodny, J. M., Thomason, L. W., and Iyer, N.: SAGE version 7.0 algorithm: application to SAGE II, Atmos. Meas. Tech., 6, 3539–3561, https://doi.org/10.5194/amt-6-3539-2013, 2013.

Davis, S. M., Rosenlof, K. H., Hassler, B., Hurst, D. F., Read, W. G., Vömel, H., Selkirk, H., Fujiwara, M., and Damadeo, R.: The Stratospheric Water and Ozone Satellite Homogenized (SWOOSH) database: a long-term database for climate studies, Earth Syst. Sci. Data, 8, 461–490, https://doi.org/10.5194/essd-8-461-2016, 2016.

Degenstein, D. A., Bourassa, A. E., Roth, C. Z., and Llewellyn, E. J.: Limb scatter ozone retrieval from 10 to 60 km using a multiplicative algebraic reconstruction technique, Atmos. Chem. Phys., 9, 6521–6529, https://doi.org/10.5194/acp-9-6521-2009, 2009.

Dubé, K., Bourassa, A., Zawada, D., Degenstein, D., Damadeo, R., Flittner, D., and Randel, W.: Accounting for the photochemical variation in stratospheric NO_2 in the SAGE III/ISS solar occultation retrieval, Atmos. Meas. Tech., 14, 557–566, https://doi.org/10.5194/amt-14-557-2021, 2021.

Dubé, K., Zawada, D., Bourassa, A., Degenstein, D., Randel, W., Flittner, D., Sheese, P., and Walker, K.: An improved OSIRIS NO_2 profile retrieval in the upper troposphere–lower stratosphere and intercomparison with ACE-FTS and SAGE III/ISS, Atmos. Meas. Tech., 15, 6163–6180, https://doi.org/10.5194/amt-15-6163-2022, 2022.

Dufour, D. G., Drummond, J. R., McElroy, C. T., Midwinter, C., Bernath, P. F., Walker, K. A., and Nowlan, C.: Simultaneous Measurements of Visible (400-700 nm) and Infrared (3.4 μm) NO2 Absorption, J. Phys. Chem. A, 110, 12 414–12 418, https://doi.org/10.1021/jp0634306, 2006.

Duncan, B. N., Strahan, S. E., Yoshida, Y., Steenrod, S. D., and Livesey, N.: Model study of the cross-tropopause transport of biomass burning pollution, Atmos. Chem. Phys., 7, 3713–3736, https://doi.org/10.5194/acp-7-3713-2007, 2007.

Dupuy, E., Walker, K. A., Kar, J., Boone, C. D., McElroy, C. T., Bernath, P. F., Drummond, J. R., Skelton, R., McLeod, S. D., Hughes, R. C., Nowlan, C. R., Dufour, D. G., Zou, J., Nichitiu, F., Strong, K., Baron, P., Bevilacqua, R. M., Blumenstock, T., Bodeker, G. E., Borsdorff, T., Bourassa, A. E., Bovensmann, H., Boyd, I. S., Bracher, A., Brogniez, C., Burrows, J. P., Catoire, V., Ceccherini, S., Chabrillat, S., Christensen, T., Coffey, M. T., Cortesi, U., Davies, J., De Clercq, C., Degenstein, D. A., De Mazière, M., Demoulin, P., Dodion, J., Firanski, B., Fischer, H., Forbes, G., Froidevaux, L., Fussen, D., Gerard, P., Godin-Beekmann, S., Goutail, F., Granville, J., Griffith, D., Haley, C. S., Hannigan, J. W., Höpfner, M., Jin, J. J., Jones, A., Jones, N. B., Jucks, K., Kagawa, A., Kasai, Y., Kerzenmacher, T. E., Kleinböhl, A., Klekociuk, A. R., Kramer, I., Küllmann, H., Kuttippurath, J., Kyrölä, E., Lambert, J.-C., Livesey, N. J., Llewellyn, E. J., Lloyd, N. D., Mahieu, E., Manney, G. L., Marshall, B. T., McConnell, J. C., McCormick, M. P., McDermid, I. S., McHugh, M., McLinden, C. A., Mellqvist, J., Mizutani, K., Murayama, Y., Murtagh, D. P., Oelhaf, H., Parrish, A., Petelina, S. V., Piccolo, C., Pommereau, J.-P., Randall, C. E., Robert, C., Roth, C., Schneider, M., Senten, C., Steck, T., Strandberg, A., Strawbridge, K. B., Sussmann, R., Swart, D. P. J., Tarasick, D. W., Taylor, J. R., Tétard, C., Thomason, L. W., Thompson, A. M., Tully, M. B., Urban, J., Vanhellemont, F., Vigouroux, C., von Clarmann, T., von der Gathen, P., von Savigny, C., Waters, J. W., Witte, J. C., Wolff, M., and Zawodny, J. M.: Validation of ozone measurements from the Atmospheric Chemistry Experiment (ACE), Atmos. Chem. Phys., 9, 287–343, https://doi.org/10.5194/acp-9-287-2009, 2009.

EOS MLS Science Team: MLS/Aura Near-Real-Time L2 Ozone (O3) Mixing Ratio V005 [data set], Greenbelt, MD, USA, Goddard Earth Sciences Data and Information Services Center (GES DISC), https://disc.gsfc.nasa.gov/datacollection/ML2O3_NRT_005.html, 2022.

Eriksson, P.: Odin/SMR Algorithm Theoretical Basis Document - Level 2 processing, Tech. rep., Department of Space, Earth and Environment, Chalmers University of Technology, http://odin.rss.chalmers.se/static/documents/PVER.pdf, 2020.

European Space Agency: Odin SMR Level 2 data products, Version 3 [data set], available at: https://odin.rss.chalmers.se/level2, last access: 10 June 2024.

European Space Agency: Envisat SCIAMACHY Level 2 - Total column densities and stratospheric profiles [SCI_OL__2P], IUP Version 3.5 [data set], ftp://scia-ftp-ds.eo.esa.int/, 2016.

European Space Agency: Envisat GOMOS Level 2 - Atmospheric constituents profiles - Gridded User Friendly Product [GOMOS_UFP_gridded], Version R/IPF 6.01 [data set], ftp://gomo-ftp-ds.eo.esa.int/, 2017.

Fischer, H., Birk, M., Blom, C., Carli, B., Carlotti, M., von Clarmann, T., Delbouille, L., Dudhia, A., Ehhalt, D., Endemann, M., Flaud, J. M., Gessner, R., Kleinert, A., Koopman, R., Langen, J., López-Puertas, M., Mosner, P., Nett, H., Oelhaf, H., Perron, G., Remedios, J.,

Ridolfi, M., Stiller, G., and Zander, R.: MIPAS: an instrument for atmospheric and climate research, Atmos. Chem. Phys., 8, 2151–2188, https://doi.org/10.5194/acp-8-2151-2008, 2008.

Flynn, L. E., Homstein, J., and Hilsenrath, E.: The ozone mapping and profiler suite (OMPS). The next generation of US ozone monitoring instruments, in: IGARSS 2004. 2004 IEEE International Geoscience and Remote Sensing Symposium, vol. 1, p. 155, https://doi.org/10.1109/IGARSS.2004.1368968, 2004.

Funke, B., López-Puertas, M., Stiller, G., v. Clarmann, T., and Höpfner, M.: A new non-LTE retrieval method for atmospheric parameters from mipas-envisat emission spectra, Adv. Space Res., 27, 1099–1104, https://doi.org/10.1016/S0273-1177(01)00169-7, 2001.

Funke, B., García-Comas, M., Glatthor, N., Grabowski, U., Kellmann, S., Kiefer, M., Linden, A., López-Puertas, M., Stiller, G. P., and von Clarmann, T.: Michelson Interferometer for Passive Atmospheric Sounding Institute of Meteorology and Climate Research/Instituto de Astrofísica de Andalucía version 8 retrieval of nitric oxide and lower-thermospheric temperature, Atmos. Meas. Tech., 16, 2167–2196, https://doi.org/10.5194/amt-16-2167-2023, 2023.

Gebhardt, C., Rozanov, A., Hommel, R., Weber, M., Bovensmann, H., Burrows, J. P., Degenstein, D., Froidevaux, L., and Thompson, A. M.: Stratospheric ozone trends and variability as seen by SCIAMACHY from 2002 to 2012, Atmos. Chem. Phys., 14, 831–846, https://doi.org/10.5194/acp-14-831-2014, 2014.

Gelaro, R., McCarty, W., Suárez, M. J., Todling, R., Molod, A., Takacs, L., Randles, C. A., Darmenov, A., Bosilovich, M. G., Reichle, R., Wargan, K., Coy, L., Cullather, R., Draper, C., Akella, S., Buchard, V., Conaty, A., da Silva, A. M., Gu, W., Kim, G.-K., Koster, R., Lucchesi, R., Merkova, D., Nielsen, J. E., Partyka, G., Pawson, S., Putman, W., Rienecker, M., Schubert, S. D., Sienkiewicz, M., and Zhao, B.: The Modern-Era Retrospective Analysis for Research and Applications, version 2 (MERRA-2), J. Climate, 30, 5419–5454, https://doi.org/10.1175/JCLI-D-16-0758.1, 2017.

Haley, C. S., Brohede, S. M., Sioris, C. E., Griffioen, E., Murtagh, D. P., McDade, I. C., Eriksson, P., Llewellyn, E. J., Bazureau, A., and Goutail, F.: Retrieval of stratospheric O_3 and NO_2 profiles from Odin Optical Spectrograph and Infrared Imager System (OSIRIS) limb-scattered sunlight measurements, J. Geophys. Res.: Atmos., 109, D16 303, https://doi.org/10.1029/2004JD004588, 2004.

Hedin, A. E.: Extension of the MSIS Thermosphere Model into the middle and lower atmosphere, J. Geophys. Res.-Space, 96, 1159–1172, https://doi.org/10.1029/90JA02125, 1991.

Hegglin, M. I., Tegtmeier, S., Anderson, J., Bourassa, A. E., Brohede, S., Degenstein, D., Froidevaux, L., Funke, B., Gille, J., Kasai, Y., Kyrölä, E. T., Lumpe, J., Murtagh, D., Neu, J. L., Pérot, K., Remsberg, E. E., Rozanov, A., Toohey, M., Urban, J., von Clarmann, T., Walker, K. A., Wang, H.-J., Arosio, C., Damadeo, R., Fuller, R. A., Lingenfelser, G., McLinden, C., Pendlebury, D., Roth, C., Ryan, N. J., Sioris, C., Smith, L., and Weigel, K.: Overview and update of the SPARC Data Initiative: comparison of stratospheric composition measurements from satellite limb sounders, Earth Syst. Sci. Data, 13, 1855–1903, https://doi.org/10.5194/essd-13-1855-2021, 2021.

Hubert, D., Lambert, J.-C., Verhoelst, T., Granville, J., Keppens, A., Baray, J.-L., Bourassa, A. E., Cortesi, U., Degenstein, D. A., Froidevaux, L., Godin-Beekmann, S., Hoppel, K. W., Johnson, B. J., Kyrölä, E., Leblanc, T., Lichtenberg, G., Marchand, M., McElroy, C. T., Murtagh, D., Nakane, H., Portafaix, T., Querel, R., Russell III, J. M., Salvador, J., Smit, H. G. J., Stebel, K., Steinbrecht, W., Strawbridge, K. B., Stübi, R., Swart, D. P. J., Taha, G., Tarasick, D. W., Thompson, A. M., Urban, J., van Gijsel, J. A. E., Van Malderen, R., von der Gathen, P., Walker, K. A., Wolfram, E., and Zawodny, J. M.: Ground-based assessment of the bias and long-term stability of 14 limb and occultation ozone profile data records, Atmos. Chem. Phys., 9, 2497–2534, https://doi.org/10.5194/amt-9-2497-2016, 2016.

Jacob, D. J.: Introduction to Atmospheric Chemistry, Princeton University Press, Princeton, NJ, USA, 1st edn., 1999.

Jaross, G., Bhartia, P. K., Chen, G., Kowitt, M., Haken, M., Chen, Z., Xu, P., Warner, J., and Kelly, T.: OMPS Limb Profiler instrument performance assessment, J. Geophys. Res.: Atmos., 119, 4399–4412, https://doi.org/10.1002/2013JD020482, 2014.

Jia, J., Rozanov, A., Ladstätter-Weißenmayer, A., and Burrows, J. P.: Global validation of SCIAMACHY limb ozone data (versions 2.9 and 3.0, IUP Bremen) using ozonesonde measurements, Atmos. Meas. Tech., 8, 3369–3383, https://doi.org/10.5194/amt-8-3369-2015, 2015.

Justus, C. G. and Johnson, D. L.: The GRAM model: Status of development and future aspects, Adv. Space Res., 19, 549–558, https://doi.org/10.1016/S0273-1177(97)00170-1, proceedings of the C1.2 and C1.3 Symposia of COSPAR Scientific Commission C, 1997.

Kar, J., McElroy, C. T., Drummond, J. R., Zou, J., Nichitiu, F., Walker, K. A., Randall, C. E., Nowlan, C. R., Dufour, D. G., Boone, C. D., Bernath, P. F., Trepte, C. R., Thomason, L. W., and McLinden, C.: Initial comparison of ozone and NO2 profiles from ACE-MAESTRO with balloon and satellite data, J. Geophys. Res.: Atmos., 112, https://doi.org/10.1029/2006JD008242, 2007.

Kerzenmacher, T. E., Walker, K. A., Strong, K., Berman, R., Bernath, P. F., Boone, C. D., Drummond, J. R., Fast, H., Fraser, A., MacQuarrie, K., Midwinter, C., Sung, K., McElroy, C. T., Mittermeier, R. L., Walker, J., and Wu, H.: Measurements of O_3, NO_2 and temperature during the 2004 Canadian Arctic ACE Validation Campaign, Geophys. Res. Lett., 32, L16S07, https://doi.org/10.1029/2005GL023032, 2005.

Kiefer, M., von Clarmann, T., Funke, B., García-Comas, M., Glatthor, N., Grabowski, U., Kellmann, S., Kleinert, A., Laeng, A., Linden, A., López-Puertas, M., Marsh, D. R., and Stiller, G. P.: IMK/IAA MIPAS temperature retrieval version 8: nominal measurements, Atmos. Meas. Tech., 14, 4111–4138, https://doi.org/10.5194/amt-14-4111-2021, 2021.

Kiefer, M., von Clarmann, T., Funke, B., García-Comas, M., Glatthor, N., Grabowski, U., Höpfner, M., Kellmann, S., Laeng, A., Linden, A., López-Puertas, M., and Stiller, G. P.: Version 8 IMK–IAA MIPAS ozone profiles: nominal observation mode, Atmos. Meas. Tech., 16, 1443–1460, https://doi.org/10.5194/amt-16-1443-2023, 2023.

Kramarova, N. and DeLand, M.: README Document for the Suomi-NPP OMPS LP L2 O3 Daily Product, https://disc.gsfc.nasa.gov/datasets/OMPS_NPP_LP_L2_O3_DAILY_2.6/summary, last accessed: 6 May 2023, 2023.

Kramarova, N. A.: OMPS-NPP L2 LP Ozone (O3) Vertical Profile swath daily Center slit V2.6 [data set], Greenbelt, MD, USA, Goddard Earth Sciences Data and Information Services Center (GES DISC), https://doi.org/10.5067/8MO7DEDYTBH7, 2023.

Kramarova, N. A., Bhartia, P. K., Jaross, G., Moy, L., Xu, P., Chen, Z., DeLand, M., Froidevaux, L., Livesey, N., Degenstein, D., Bourassa, A., Walker, K. A., and Sheese, P.: Validation of ozone profile retrievals derived from the OMPS LP version 2.5 algorithm against correlative satellite measurements, Atmos. Meas. Tech., 11, 2837–2861, https://doi.org/10.5194/amt-11-2837-2018, 2018.

Kremser, S., Thomason, L. W., and Bird, L. J.: Simplified SAGE II ozone data usage rules, Earth Syst. Sci. Data, 12, 1419–1435, https://doi.org/10.5194/essd-12-1419-2020, 2020.

Kyrölä, E., Tamminen, J., Sofieva, V., Bertaux, J. L., Hauchecorne, A., Dalaudier, F., Fussen, D., Vanhellemont, F., Fanton d'Andon, O., Barrot, G., Guirlet, M., Mangin, A., Blanot, L., Fehr, T., Saavedra de Miguel, L., and Fraisse, R.: Retrieval of atmospheric parameters from GOMOS data, Atmos. Chem. Phys., 10, 11 881–11 903, https://doi.org/10.5194/acp-10-11881-2010, 2010.

Kyrölä, E., Tamminen, J., Leppelmeier, G. W., Sofieva, V., Hassinen, S., Bertaux, J. L., Hauchecorne, A., Dalaudier, F., Cot, C., Korablev, O., Fanton d'Andon, O., Barrot, G., Mangin, A., Théodore, B., Guirlet, M., Etanchaud, F., Snoeij, P., Koopman, R., Saavedra, L., Fraisse, R., Fussen, D., and Vanhellemont, F.: GOMOS on Envisat: an overview, Adv. Space Res., 33, 1020–1028, https://doi.org/10.1016/S0273-1177(03)00590-8, 2004.

Kyrölä, E., Sofieva, V., Hakkarainen, J., and Tamminen, J.: Product Quality Readme File for GOMOS ALGOM User Friendly Dataset, https://earth.esa.int/eogateway/documents/20142/1519072/ALGOM-GOMOS-user-friendly-dataset-readme.pdf, accessed on 11 May 2023, 2017.

Lacis, A. A., Wuebbles, D. J., and Logan, J. A.: Radiative forcing of climate by changes in the vertical distribution of ozone, J. Geophys. Res.: Atmos., 95, 9971–9981, https://doi.org/10.1029/JD095iD07p09971, 1990.

Laeng, A., von Clarmann, T., Stiller, G., Dinelli, B. M., Dudhia, A., Raspollini, P., Glatthor, N., Grabowski, U., Sofieva, V., Froidevaux, L., Walker, K. A., and Zehner, C.: Merged ozone profiles from four MIPAS processors, Atmos. Meas. Tech., 10, 1511–1518, https://doi.org/10.5194/amt-10-1511-2017, 2017.

Livesey, N. J., Read, W. G., Wagner, P. A., Froidevaux, L., Santee, M. L., Schwartz, M. J., Lambert, A. ad Millán Valle, L. F., Pumphrey, H. C., Manney, G. L., Fuller, R. A., Jarnot, R. F., Knosp, B. W., and Lay, R. R.: Earth Observing System (EOS) Aura Microwave Limb Sounder (MLS) Version 5.0x Level 2 and 3 data quality and description document., Tech. rep., , Jet Propulsion Laboratory, https://mls.jpl.nasa.gov/data/v5-0_data_quality_document.pdf, 2022.

Llewellyn, E. J., Lloyd, N. D., Degenstein, D. A., Gattinger, R. L., Petelina, S. V., Bourassa, A. E., Wiensz, J. T., Ivanov, E. V., McDade, I. C., Solheim, B. H., McConnell, J. C., Haley, C. S., von Savigny, C., Sioris, C. E., McLinden, C. A., Griffioen, E., Kaminski, J., Evans, W. F. J., Puckrin, E., Strong, K., Wehrle, V., Hum, R. H., Kendall, D. J. W., Matsushita, J., Murtagh, D. P., Brohede, S., Stegman, J., Witt, G., Barnes, G., Payne, W. F., Piché, L., Smith, K., Warshaw, G., Deslauniers, D.-L., Marchand, P., Richardson, E. H., King, R. A., Wevers, I., McCreath, W., Kyrölä, E., Oikarinen, L., Leppelmeier, G. W., Auvinen, H., Mégie, G., Hauchecorne, A., Lefèvre, F., de La Nöe, J., Ricaud, P., Frisk, U., Sjoberg, F., von Schéele, F., and Nordh, L.: The OSIRIS instrument on the Odin spacecraft, Can. J. Phys., 82, 411–422, https://doi.org/10.1139/p04-005, 2004.

Loew, A., Bell, W., Brocca, L., Bulgin, C. E., Burdanowitz, J., Calbet, X., Donner, R. V., Ghent, D., Gruber, A., Kaminski, T., Kinzel, J., Klepp, C., Lambert, J.-C., Schaepman-Strub, G., Schröder, M., and Verhoelst, T.: Validation practices for satellite-based Earth observation data across communities, Rev. Geophys., 55, 779–817, https://doi.org/10.1002/2017RG000562, 2017.

MAESTRO: MAESTRO Version 4 Level 2 Data [data set], available at: https://databace.scisat.ca/level2/, last access: 10 June 2024.

Manney, G. L., Santee, M. L., and Zinoviev, N. S.: Unprecedented Arctic ozone loss in 2011, Nature, 478, 469–475, https://doi.org/10.1038/nature10556, 2011.

Mauldin III, L. E., Zaun, N. H., McCormick Jr., M. P., Guy, J. H., and Vaughn, W. r.: Stratospheric Aerosol And Gas Experiment II Instrument: A Functional Description, Opt. Eng., 24, 242 307, https://doi.org/10.1117/12.7973473, 1985.

Mauldin III, L. E., Salikhov, R., Habib, S., Vladimirov, A. G., Carraway, D., Petrenko, G., and Comella, J.: Meteor-3M(1)/Stratospheric Aerosol and Gas Experiment III (SAGE III) jointly sponsored by the National Aeronautics and Space Administration and the Russian Space Agency, in: Optical Remote Sensing of the Atmosphere and Clouds, edited by Wang, J., Wu, B., Ogawa, T., and Guan, Z., vol. 3501, pp. 355–365, International Society for Optics and Photonics, SPIE, https://doi.org/10.1117/12.317767, 1998.

McCormick, M. P.: Sage II: An overview, Adv. Space Res., 7, 219–226, https://doi.org/10.1016/0273-1177(87)90151-7, 1987.

McCormick, M. P., Zawodny, J. M., Veiga, R. E., Larsen, J. C., and Wang, P. H.: An overview of sage I and II ozone measurements, Planet. Space Sci., 37, 1567–1586, https://doi.org/10.1016/0032-0633(89)90146-3, 1989.

McCormick, M. P., Lei, L., Hill, M. T., Anderson, J., Querel, R., and Steinbrecht, W.: Early results and validation of SAGE III-ISS ozone profile measurements from onboard the International Space Station, Atmos. Meas. Tech., 13, 1287–1297, https://doi.org/10.5194/amt-13-1287-2020, 2020.

McElroy, C. T., Nowlan, C. R., Drummond, J. R., Bernath, P. F., Barton, D. V., Dufour, D. G., Midwinter, C., Hall, R. B., Ogyu, A., Ullberg, A., Wardle, D. I., Kar, J., Zou, J., Nichitiu, F., Boone, C. D., Walker, K. A., and Rowlands, N.: The ACE-MAESTRO instrument on SCISAT: Description, performance, and preliminary results, Appl. Optics., 46, 4341–4356, https://doi.org/10.1364/AO.46.004341, 2007.

MIPAS IMK-IAA: Level 2 Data, Version 8, IMK-IAA, MIPAS [data set], available at: https://imk-asf-mipas.imk.kit.edu/, last access: 11 June 2024.

Molod, A., Takacs, L., Suarez, M., and Bacmeister, J.: Development of the GEOS-5 atmospheric general circulation model: evolution from MERRA to MERRA2, Geosci. Model Dev., 8, 1339–1356, https://doi.org/10.5194/gmd-8-1339-2015, 2015.

Murtagh, D., Frisk, U., Merino, F., Ridal, M., Jonsson, A., Stegman, J., Witt, G., Eriksson, P., Jiménez, C., Megie, G., de la Noë, J., Ricaud, P., Baron, P., Pardo, J. R., Hauchcorne, A., Llewellyn, E. J., Degenstein, D. A., Gattinger, R. L., Lloyd, N. D., Evans, W. F. J., McDade, I. C., Haley, C. S., Sioris, C., von Savigny, C., Solheim, B. H., McConnell, J. C., Strong, K., Richardson, E. H., Leppelmeier, G. W., Kyrölä, E., Auvinen, H., and Oikarinen, L.: An overview of the Odin atmospheric mission, Can. J. Phys., 80, 309–319, https://doi.org/10.1139/p01-157, 2002.

Murtagh, D., Skyman, A., Rydberg, B., and Eriksson, P.: Odin/SMR Product Validation and Evolution Report, Tech. rep., Department of Space, Earth and Environment, Chalmers University of Technology, http://odin.rss.chalmers.se/static/documents/PVER.pdf, 2020.

NASA/LARC/SD/ASDC: SAGE III/ISS L2 Solar Event Species Profiles (HDF5) V053 [data set], https://doi.org/10.5067/ISS/SAGEIII/SOLAR_HDF5_L2-V5.3, last access: 11 June 2024.

NASA/LARC/SD/ASDC: SAGE III Meteor-3M L2 Solar Event Species Profiles (HDF-EOS) V004 [data set], https://doi.org/10.5067/M3M/SAGEIII/SOLAR_HDF-EOS_L2-V4.0, 2009.

NASA/LARC/SD/ASDC: Stratospheric Aerosol and Gas Experiment (SAGE) II Version 7.0 Aerosol, O_3, NO_2 and H_2O Profiles in binary format [data set], https://doi.org/10.5067/ERBS/SAGEII/SOLAR_BINARY_L2-V7.0, 2012.

Nielsen, J. E., Pawson, S., Molod, A., Auer, B., da Silva, A. M., Douglass, A. R., Duncan, B., Liang, Q., Manyin, M., Oman, L. D., Putman, W., Strahan, S. E., and Wargan, K.: Chemical Mechanisms and Their Applications in the Goddard Earth Observing System (GEOS) Earth System Model, J. Adv. Model Earth Sy., 9, 3019–3044, https://doi.org/10.1002/2017MS001011, 2017.

OSIRIS: OSIRIS Version 7.2 Level 2 [data set], available at: ftp://odin-osiris.usask.ca/, last access: 10 June 2024.

Prather, M. J.: Ozone in the upper stratosphere and mesosphere, J. Geophys. Res.-Oceans, 86, 5325–5338, https://doi.org/https://doi.org/10.1029/JC086iC06p05325, 1981.

Pérot, K., Eriksson, P., Murtagh, D., and Rydberg, B.: Odin/SMR L2 data - format and overview, Tech. rep., Department of Space, Earth and Environment, Chalmers University of Technology, http://odin.rss.chalmers.se/static/documents/L2_DATA.pdf, 2020.

Rault, D. F. and Loughman, R. P.: The OMPS Limb Profiler Environmental Data Record Algorithm Theoretical Basis Document and Expected Performance, IEEE T. Geosci. Remote, 51, 2505–2527, https://doi.org/10.1109/TGRS.2012.2213093, 2013.

Rienecker, M. M., Suarez, M. J., Gelaro, R., Todling, R., Bacmeister, J., Liu, E., Bosilovich, M. G., Schubert, S. D., Takacs, L., Kim, G.-K., Bloom, S., Chen, J., Collins, D., Conaty, A., da Silva, A., Gu, W., Joiner, J., Koster, R. D., Lucchesi, R., Molod, A., Owens, T., Pawson, S., Pegion, P., Redder, C. R., Reichle, R., Robertson, F. R., Ruddick, A. G., Sienkiewicz, M., and Woollen, J.: MERRA: NASA's Modern-Era Retrospective Analysis for Research and Applications, J. Climate, 24, 3624–3648, https://doi.org/10.1175/JCLI-D-11-00015.1, 2011.

SAGE III ATBD: SAGE III Algorithm Theoretical Basis Document (ATBD) Solar and Lunar Algorithm version 2.1, Tech. rep., NASA Langley Research Center (LaRC), https://eospso.gsfc.nasa.gov/sites/default/files/atbd/atbd-sage-solar-lunar.pdf, 2002.

SAGE III/ISS Data Products User's Guide: Stratospheric Aerosol and Gas Experiment on the International Space Station (SAGE III/ISS) Data Products User's Guide, https://asdc.larc.nasa.gov/documents/sageiii-iss/guide/DPUG_G3B_v05.30.pdf, accessed on 18 May 2023, 2023.

Sakazaki, T., Fujiwara, M., Mitsuda, C., Imai, K., Manago, N., Naito, Y., Nakamura, T., Akiyoshi, H., Kinnison, D., Sano, T., Suzuki, M., and Shiotani, M.: Diurnal ozone variations in the stratosphere revealed in observations from the Superconducting Submillimeter-Wave Limb-Emission Sounder (SMILES) on board the International Space Station (ISS), J. Geophys. Res.: Atmos., 118, 2991–3006, https://doi.org/10.1002/jgrd.50220, 2013.

Sakazaki, T., Shiotani, M., Suzuki, M., Kinnison, D., Zawodny, J. M., McHugh, M., and Walker, K. A.: Sunset–sunrise difference in solar occultation ozone measurements (SAGE II, HALOE, and ACE–FTS) and its relationship to tidal vertical winds, Atmos. Chem. Phys., 15, 829–843, https://doi.org/10.5194/acp-15-829-2015, 2015.

Serdyuchenko, A., Gorshelev, V., Weberand, M., and Burrows, J. P.: New broadband high-resolution ozone absorption cross-sections, Spectrosc. Eur., 23, 14–17, https://www.spectroscopyeurope.com/article/new-broadband-high-resolution-ozone-absorption-cross-sections, 2011.

Sheese, P. and Walker, K.: Data Quality Flags for ACE-FTS Level 2 Version 4.1/4.2 Data Set, Borealis, V30, [data set], https://doi.org/10.5683/SP2/BC4ATC, 2023a.

Sheese, P. and Walker, K.: Data Quality Flags for ACE-FTS Level 2 Version 5.2 Data Set, Borealis, V3, [data set], https://doi.org/10.5683/SP3/NAYNFE, 2023b.

Sheese, P. E., Boone, C. D., and Walker, K. A.: Detecting physically unrealistic outliers in ACE-FTS atmospheric measurements, Atmos. Meas. Tech., 8, 741–750, https://doi.org/10.5194/amt-8-741-2015, 2015.

Sheese, P. E., Walker, K. A., Boone, C. D., McLinden, C. A., Bernath, P. F., Bourassa, A. E., Burrows, J. P., Degenstein, D. A., Funke, B., Fussen, D., Manney, G. L., McElroy, C. T., Murtagh, D., Randall, C. E., Raspollini, P., Rozanov, A., Russell III, J. M., Suzuki, M., Shiotani, M., Urban, J., von Clarmann, T., and Zawodny, J. M.: Validation of ACE-FTS version 3.5 NO_y species profiles using correlative satellite measurements, Atmos. Meas. Tech., 9, 5781–5810, https://doi.org/10.5194/amt-9-5781-2016, 2016.

Sheese, P. E., Walker, K. A., Boone, C. D., Bernath, P. F., Froidevaux, L., Funke, B., Raspollini, P., and von Clarmann, T.: ACE-FTS ozone, water vapour, nitrous oxide, nitric acid, and carbon monoxide profile comparisons with MIPAS and MLS, J. Quant. Spectrosc. Ra., 186, 63–80, https://doi.org/10.1016/j.jqsrt.2016.06.026, satellite Remote Sensing and Spectroscopy: Joint ACE-Odin Meeting, October 2015, 2017.

Sheese, P. E., Walker, K. A., Boone, C. D., Degenstein, D. A., Kolonjari, F., Plummer, D., Kinnison, D. E., Jöckel, P., and von Clarmann, T.: Model estimations of geophysical variability between satellite measurements of ozone profiles, Atmos. Meas. Tech., 14, 1425–1438, https://doi.org/10.5194/amt-14-1425-2021, 2021.

Sheese, P. E., Walker, K. A., Boone, C. D., Bourassa, A. E., Degenstein, D., Froidevaux, L., McElroy, C. T., Murtagh, D., Russell III, J. M., and Zou, J.: Assessment of the quality of ACE-FTS stratospheric ozone data, Atmos. Meas. Tech., 15, 1233–1249, https://doi.org/10.5194/amt-15-1233-2022, 2022.

Sioris, C. E., Zou, J., Plummer, D. A., Boone, C. D., McElroy, C. T., Sheese, P. E., Moeini, O., and Bernath, P. F.: Upper tropospheric water vapour variability at high latitudes – Part 1: Influence of the annular modes, Atmos. Chem. Phys., 16, 3265–3278, https://doi.org/10.5194/acp-16-3265-2016, 2016.

Sofieva, V. F., Szeląg, M., Tamminen, J., Kyrölä, E., Degenstein, D., Roth, C., Zawada, D., Rozanov, A., Arosio, C., Burrows, J. P., Weber, M., Laeng, A., Stiller, G. P., von Clarmann, T., Froidevaux, L., Livesey, N., van Roozendael, M., and Retscher, C.: Measurement report: regional trends of stratospheric ozone evaluated using the MErged GRIdded Dataset of Ozone Profiles (MEGRIDOP), Atmos. Chem. Phys., 21, 6707–6720, https://doi.org/10.5194/acp-21-6707-2021, 2021.

SPARC-DI: The SPARC (Stratospheric Processes And their Role in Climate) Data Initiative: Assessment of stratospheric trace gas and aerosol climatologies from satellite limb sounders, SPARC Report No. 8, WCRP-05/2017, https://doi.org/10.3929/ethz-a-010863911, 2017.

Strahan, S. E., Duncan, B. N., and Hoor, P.: Observationally derived transport diagnostics for the lowermost stratosphere and their application to the GMI chemistry and transport model, Atmos. Chem. Phys., 7, 2435–2445, https://doi.org/10.5194/acp-7-2435-2007, 2007.

Strode, S.: Diurnal Scaling Factors, NASA [data set], https://avdc.gsfc.nasa.gov/pub/data/project/GMI_SF/, 2021.

Strode, S. A., Taha, G., Oman, L. D., Damadeo, R., Flittner, D., Schoeberl, M., Sioris, C. E., and Stauffer, R.: SAGE III/ISS ozone and NO_2 validation using diurnal scaling factors, Atmos. Meas. Tech., 15, 6145–6161, https://doi.org/10.5194/amt-15-6145-2022, 2022.

Tamminen, J., Kyrölä, E., Sofieva, V. F., Laine, M., Bertaux, J.-L., Hauchecorne, A., Dalaudier, F., Fussen, D., Vanhellemont, F., Fanton-d'Andon, O., Barrot, G., Mangin, A., Guirlet, M., Blanot, L., Fehr, T., Saavedra de Miguel, L., and Fraisse, R.: GOMOS data characterisation and error estimation, Atmos. Chem. Phys., 10, 9505–9519, https://doi.org/10.5194/acp-10-9505-2010, 2010.

Thomason, L. W., Moore, J. R., Pitts, M. C., Zawodny, J. M., and Chiou, E. W.: An evaluation of the SAGE III version 4 aerosol extinction coefficient and water vapor data products, Atmos. Chem. Phys., 10, 2159–2173, https://doi.org/10.5194/acp-10-2159-2010, 2010.

Urban, J., Lautié, N., Le Flochmoën, E., Jiménez, C., Eriksson, P., de La Noë, J., Dupuy, E., Ekström, M., El Amraoui, L., Frisk, U., Murtagh, D., Olberg, M., and Ricaud, P.: Odin/SMR limb observations of stratospheric trace gases: Level 2 processing of ClO, N2O, HNO3, and O3, J. Geophys. Res.: Atmos., 110, https://doi.org/10.1029/2004JD005741, 2005.

Vandaele, A. C., Hermans, C., Fally, S., Carleer, M., Colin, R., Mérienne, M.-F., Jenouvrier, A., and Coquart, B.: High-resolution Fourier transform measurement of the NO2 visible and near-infrared absorption cross sections: Temperature and pressure effects, J. Geophys. Res.: Atmos., 107, ACH 3–1–ACH 3–12, https://doi.org/10.1029/2001JD000971, 2002.

von Clarmann, T., Glatthor, N., Grabowski, U., Höpfner, M., Kellmann, S., Kiefer, M., Linden, A., Tsidu, G. M., Milz, M., Steck, T., Stiller, G. P., Wang, D. Y., Fischer, H., Funke, B., Gil-López, S., and López-Puertas, M.: Retrieval of temperature and tangent altitude pointing from limb emission spectra recorded from space by the Michelson Interferometer for Passive Atmospheric Sounding (MIPAS), J. Geophys. Res.: Atmos., 108, https://doi.org/10.1029/2003JD003602, 2003.

von Clarmann, T., Höpfner, M., Kellmann, S., Linden, A., Chauhan, S., Funke, B., Grabowski, U., Glatthor, N., Kiefer, M., Schieferdecker, T., Stiller, G. P., and Versick, S.: Retrieval of temperature, H_2O, O_3, HNO_3, CH_4, N_2O, $ClONO_2$ and ClO from MIPAS reduced resolution nominal mode limb emission measurements, Atmos. Meas. Tech., 2, 159–175, https://doi.org/10.5194/amt-2-159-2009, 2009.

Wang, H. J., Cunnold, D. M., Thomason, L. W., Zawodny, J. M., and Bodeker, G. E.: Assessment of SAGE version 6.1 ozone data quality, J. Geophys. Res.: Atmos., 107, ACH 8–1–18, https://doi.org/10.1029/2002JD002418, 2002.

Wang, H.-J., Cunnold, D. M., Trepte, C., Thomason, L. W., and Zawodny, J. M.: SAGE III solar ozone measurements: Initial results, Geophys. Res. Lett., 33, https://doi.org/10.1029/2005GL025099, 2006.

Wang, H. J. R., Damadeo, R., Flittner, D., Kramarova, N., Taha, G., Davis, S., Thompson, A. M., Strahan, S., Wang, Y., Froidevaux, L., Degenstein, D., Bourassa, A., Steinbrecht, W., Walker, K. A., Querel, R., Leblanc, T., Godin-Beekmann, S., Hurst, D., and Hall, E.: Validation of SAGE III/ISS Solar Occultation Ozone Products With Correlative Satellite and Ground-Based Measurements, J. Geophys. Res.: Atmos., 125, e2020JD032 430, https://doi.org/0.1029/2020JD032430, 2020.

Waters, J. W., Froidevaux, L., Harwood, R. S., Jarnot, R. F., Pickett, H. M., Read, W. G., Siegel, P. H., Cofield, R. E., Filipiak, M. J., Flower, D. A., Holden, J. R., Lau, G. K., Livesey, N. J., Manney, G. L., Pumphrey, H. C., Santee, M. L., Wu, D. L., Cuddy, D. T., Lay, R. R., Loo, M. S., Perun, V. S., Schwartz, M. J., Stek, P. C., Thurstans, R. P., Boyles, M. A., Chandra, K. M., Chavez, M. C., Chen, G.-S., Chudasama, B. V., Dodge, R., Fuller, R. A., Girard, M. A., Jiang, J. H., Jiang, Y., Knosp, B. W., LaBelle, R. C., Lam, J. C., Lee, K. A., Miller, D., Oswald, J. E., Patel, N. C., Pukala, D. M., Quintero, O., Scaff, D. M., Van Snyder, W., Tope, M. C., Wagner, P. A., and Walch, M. J.: The Earth observing system microwave limb sounder (EOS MLS) on the aura Satellite, IEEE T. Geosci. Remote, 44, 1075–1092, https://doi.org/10.1109/TGRS.2006.873771, 2006.